Co-funded by the

MIND

Microbiology In Nuclear waste Disposal

(GRANT AGREEMENT: 661880)

DELIVERABLE 2.16

Microbial activity and the physical, chemical and transport properties of bentonite buffer

Editors:

Simon Gregory, UKRI BGS
Lorraine Field, UKRI BGS
Kay Green, UKRI BGS
Jon Harrington, UKRI BGS
Simon Kemp, UKRI BGS
Keith Bateman, NERC BGS
Simon Kemp, UKRI BGS
Hayden Haynes, University of Manchester
Jon Lloyd, University of Manchester

Date of issue of this report:

This project has received funding from the Euratom research and training programme 2014-2018 under Grant Agreement no. 661880		
Dissemination Level		
PU	Public	**PU**
PP	Restricted to other programme participants (including the Commission)	
RE	Restricted to a group specified by the partners of the MIND project	
CO	Confidential, only for partners of the MIND project	

Publishable Summary

A series of experiments have been carried out into microbial survival and activity in compacted FEBEX bentonite compressed to dry densities of 1200 kg m^{-1} and 1400 kg m^{-1}. Samples were prepared containing steel chips and an artificial groundwater. Samples were then inserted into a constant volume axial flow vessel. The use of this set up allowed the simultaneous investigation of interactions between the steel, bentonite and microorganisms, whilst also monitoring bentonite permeability and swelling pressures. By using this set up the influence of microorganisms on the performance of the bentonite as a buffer material could be investigated. The bentonite was sterilised by irradiation, and sulphate reducing bacteria were reintroduced into half the tests so that the influence of microbial activity could be investigated. The number of sulphate reducing bacteria, anaerobic and aerobic heterotrophic bacteria monitored in all tests. Bacteria were seen to persist and increase in inoculated tests while bacterial numbers remained low in uninoculated tests. Previous reports of higher microbial survival in lower density bentonite samples have been confirmed for FEBEX bentonite, with survival and growth detected in samples with an initial dry density of 1200 kg m^{-1} and 1400 kg m^{-3}. This indicates that in FEBEX bentonite microorganisms survive in the upper range of dry densities reported for microbial survival. Initial tests run using samples with a dry density of 1400 kg m^{-1} suggested that the presence of microorganisms is associated with particular iron phases and the development of aragonite crystals. The basal spacing of bentonite increased during three of these tests, indicating replacement of monovalent cations by divalent ones in experiments. Lower density experiments did not show this same pattern; iron and calcium alteration was observed in both tests at 1200 kg m^{-1} with greatest alteration being observed in the uninoculated test along with iron sulphide precipitation. In the lower density samples the shift from monovalent to divalent cations was much less pronounced.

In all tests, permeability was lower in the inoculated sample, and in the low-density tests (1200 kg m^{-3}) a 20% reduction in permeability was observed in inoculated samples. Other than this reduction of permeability there was no consistent pattern associated with the presence or absence of microorganisms. However, the possibility that microorganisms could influence the mineralogical and petrological character of the bentonite has been highlighted. These changes could affect its performance as a barrier material and further studies need to be undertaken to confirm the role of microorganisms in steel corrosion and its impact on bentonite behaviour.

Contents

1 Introduction

The survival and activity of microorganisms in the extreme environments generated around a geological disposal facility (GDF has been established in many studies (Stroes-Gascoyne and West, 1997; Humphreys *et al.*, 2010; Libert *et al.*, 2013), but further work is required to fully determine the impacts on the GDF safety case. Microbial activity in and around a GDF could affect metal corrosion, bentonite swelling capacity and radionuclide mobility. The focus of this report is to present experimental data acquired in the MIND project by the British Geological Survey (BGS) on the influence of microbial activity within bentonite on the physical-, chemical- and transport-properties of bentonite clay.

Microorganisms are present both in natural clay host rocks (Boivin-Jahns and Ruimy, 1996; Deniau *et al.*, 2001; Urios *et al.*, 2012; Lopez-Fernandez *et al.*, 2015; Bagnoud *et al.*, 2016) and in industrial bentonites that will be used as buffer materials in the design of a GDF (Masurat *et al.*, 2010a; Wouters *et al.*, 2013). In clay formations or compacted bentonite, microbial biomass and activity is likely to be limited, due to a combination of factors including limited pore spaces, accessible carbon sources and water availability (Leupin *et al.*, 2017) but studies show that viable microbes persist within natural clay formations and under repository conditions (Motamedi *et al.*, 1996; Pedersen *et al.*, 2000; Bengtsson and Pedersen, 2017), though many of these cells may be surviving in dormant states or as spores (Pedersen *et al.*, 2000; Stroes-Gascoyne *et al.*, 2010). Microbial survival in compacted bentonite has been shown to be dependent on the density of compaction. For Wyoming MX-80 bentonite between 1250kg m^{-3} to 1600 kg m^{-3} dry density has been suggested as the limit to microbial survival (Stroes-Gascoyne *et al.*, 2010; Smart *et al.*, 2017). Other studies have put the limit to survival of sulphate reducing bacteria (SRB) between 1900 kg m^{-3} to 2100 kg m^{-3} wet density Wyoming MX80 (equivalent to a dry density in the region of 1400 kg m^{-3} to 1575 kg m^{-3}) (Pedersen *et al.*, 2000; Masurat *et al.*, 2010b). In comparison, SRB remained viable in Rokle and iron-poor Gaomiaozi up to the maximum tested wet density of 1950 kg m^{-3} (approximately 1400 kg m^{-3} dry density), and lactate consumption and the activity of SRB decreased with increasing density (Bengtsson *et al.*, 2017). The limit to bacterial sulphide production is considered to be 1870 kg m^{-3} in Calcigel and Wyoming MX80 and 1830 kg m^{-3} in Asha (equivalent to approximately 1300 kg m^{-3}) (Bengtsson and Pedersen, 2017). Recent work carried out within the MIND project found *Desulfotomaculum* species dominated SRB enrichment cultures from FEBEX bentonite, with some *Desulfosporosinus* species also present (Haynes *et al.*, 2018). In contrast, *Desulfosporosinus dominated* the other bentonites tested (southern (Mississippi, USA), western (Wyoming, USA) bentonite and a commercial bentonite (Thermo Fisher Scientific Waltham, MA, USA)). Generally, *Desulfotomaculum* became enriched compared to *Desulfosporosinus* when exposed to high pressure (74 MPa, 30 s) and irradiation (1000 Gy, 24.17 Gy min−1) but showed diminished viability after heat treatment (90 °C, 24 h), although in some cases this varied depending on the type of bentonite. Considering the wider microbial community, the work by Haynes et al (2019) noted an increase in the number of Gram-positive spore formers in response to stresses. It was also observed that the different microbial communities in each bentonite was important for the survival of SRB when stress was applied.

In a variety of environments, such as soils or depleted hydrocarbon reservoirs, the actions of bacteria have been shown to reduce the swelling capacity of clays (Kostka *et al.*, 1999; Cui *et al.*, 2018), and although it has been suggested to occur in the context of radioactive waste repositories (Perdrial *et al.*, 2009; Esnault *et al.*, 2013), the extent to which this can occur in compacted bentonite within a GDF environment is not well understood. A potential mechanism for this is thought to be linked to microbial iron reduction resulting in the conversion of smectite to illite (Mulligan *et al.*, 2009; Perdrial *et al.*, 2009). The associated loss of swelling capacity has the potential to negatively impact on the effectiveness of the bentonite to act as a barrier to movement of groundwater and radionuclides.

The MIND-project has received funding from the European Union's Euratom research and training program (Horizon2020) under grant agreement 661880.

In addition to altering clay properties, microorganisms have been implicated in corrosion of metals used, for example, in canister material (Hajj *et al.*, 2010; Féron and Crusset, 2014; Rajala *et al.*, 2015, 2017). Corrosion of metals produces hydrogen which is a highly energetic electron donor important for microbial activity in many natural and engineered subsurface environments (Gregory *et al.*, 2019).As many microorganisms e.g. SRB and acetate producers, can use hydrogen as an electron donor, hydrogen scavenging by microorganisms may accelerate anaerobic corrosion of iron as follows: Hydrogen generated by microbial or abiotic corrosion fuels the metabolism of microorganisms implicated in corrosion because their metabolic products are known to be corrosive (e.g. sulphide is corrosive for both iron and copper and acetate can cause stress cracking in copper). These interact with metals in the vicinity of the active microorganism and increase corrosion, liberating more hydrogen, which is then available to support the hydrogenotrophic microbial community.

Consequently, because of the potential impacts on metal and clay properties, there is a need to understand the limits to microbial growth in bentonites and the potential for microbial activity to affect the swelling behaviour of the clay and metal corrosion. This report describes the impact of microbe-clay-radionuclide interactions in laboratory experiments designed to investigate microbial survival and activity in compacted bentonites and how this affects the physical-, chemical- and transport-properties of the clay.

2 Methods

2.1 Sample and media preparation

2.1.1 Selection of bentonites

Powdered FE bentonite from the full-scale engineered barriers experiment (FEBEX) (obtained from NAGRA) was used for all experiments. This was irradiated at Manchester University's Dalton Facility, Cumbria (dose rate range of 30 Gy to 53.1 Gy) prior to use. No microbial growth was observed from treated bentonite in nutrient broth in aerobic or anaerobic conditions.

2.1.2 Bentonite sample preparation

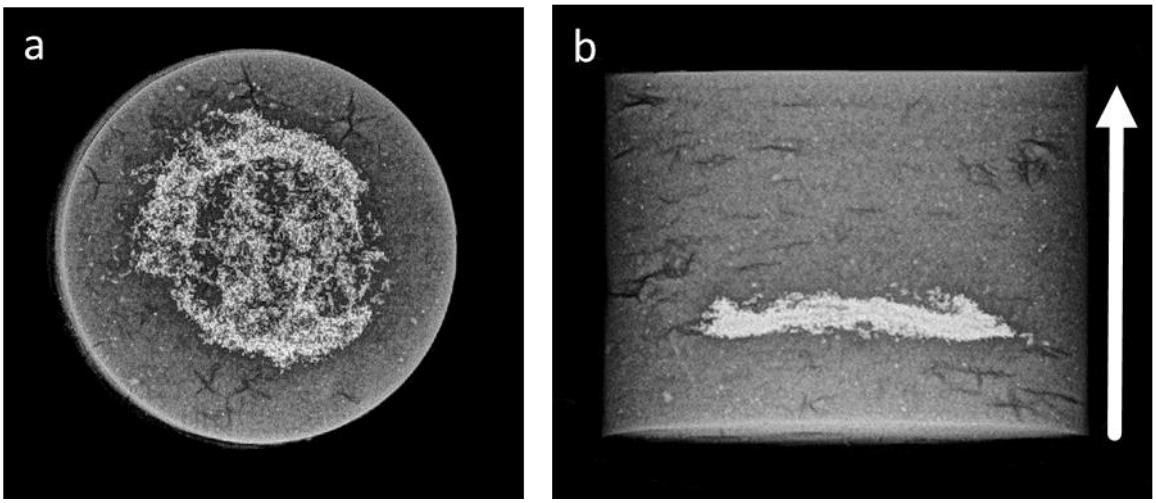

Figure 1 *X-ray of prepared sample (note this sample was an early test sample, not used in any experiment). Longer compression times were used for experimental samples which resulted in a more homogenous clay appearance) (b) shows orientation of sample and direction of flow when in the CVAF*

Table 1 shows the basic physical properties of each test specimen. As preserved sample material was required for post-mortem analysis it was not possible to oven dry the sample (in order to determine

The MIND-project has received funding from the European Union's Euratom research and training program (Horizon2020) under grant agreement 661880.

the basic geotechnical properties). Instead, bulk density was estimated by simply subtracting the mass of steel from the wet-weight of the sample which was then divided by the volume.

Table 1 Basic physical properties of the test specimens.

Specimen number	Inoculated with SRB enrichment	Lactate	Mass metal (g)	Length (mm)	Diameter (mm)	Estimated bulk density (kg m^{-3})
BUG021	No	No	4.73	47.50	49.96	1834
BUG022	Yes	No	4.98	47.79	49.95	1841
BUG023	No	Yes	5.00	51.72	49.82	1855
BUG024	Yes	Yes	5.00	50.95	50.05	1852
BUG025	No	Yes	5.00	48.54	49.99	1756
BUG026	Yes	Yes	5.00	48.39	50.01	1762
BUG027	No	Yes	5.05	51.00	50.02	1859
BUG028	Yes	Yes	5.00	50.77	50.04	1864

2.1.3 Media and artificial groundwater preparation

Table 2 Composition of media and artificial groundwater used in this study

Media/ groundwater	Use	Composition (all masses shown per litre)
Artificial groundwater	Sample preparation, experimental fluid	33.04mg $Ca(NO_3)_2.4H_2O$; 0.22mg KF; 8.73mg NaCl; 7.56mg $(NH_4)_2SO_4$; 12.36mg NaF
PTYG medium	Enumeration of aerobic and anaerobic heterotrophs	5.00 g Peptone; 5.00 g Tryptone; 5.00 g Yeast extract; 10g Glucose; 0.60 g $MgSO_4.7\ H_2O$; 0.06 g $CaCl_2$. pH 7.0 (DSMZ recipe 914)
Postgate's medium B	Enumeration of SRB	0.50 g KH_2PO4; 1.00 g NH_4Cl; 1 g $CaSO_4$; 2 g $MgSO_4.7H_2O$; 3.5 ml 60% w/w Sodium lactate solution; 1 g Yeast extract; 0.1 g Ascorbic Acid; 0.1g Thioglycolic acid; 0.5g $FeSO_4.7H_2O$. Prepared using tap water. pH 7.0-7.5 (Postgate, 1979)

An artificial groundwater was prepared based on Grimsel groundwater (composition in Table 2). This groundwater was used for preparation and hydration of samples and was used as the fluid flowing across samples in tests. The groundwater in experiments containing lactate (Table 1) was amended with sodium lactate to a final concentration of 10mM. For inoculated experiments (Table 1), the sample was prepared with groundwater containing a sulphate-reducing bacteria (SRB) enrichment culture. This was prepared by inoculating approximately 150 ml Postgate's medium B (Table 2) with 1 g un-irradiated FE bentonite and incubating in sealed glass bottles in an anoxic environment (95% N_2, 5% H_2 at 35˚C). After the appearance of a black precipitate, indicative of sulphate reduction, enrichment cultures were centrifuged and resuspended in artificial groundwater, which was then used to hydrate the inoculated samples.

The MIND-project has received funding from the European Union's Euratom research and training program (Horizon2020) under grant agreement 661880.

Media used for enumerations of different bacterial groups is shown in Table 2. All media and groundwater were autoclaved at 121°C for 15 minutes.

2.2 Experimental procedures

2.2.1 Set-up of constant volume axial flow apparatus

All experiments were run as flow experiments in constant volume axial flow (CVAF) apparatus designed to examine the sensitivity of swelling pressure and permeability to the corrosion of iron compacted within the bentonite clay (Figure 2 and Figure 3). Full description of this apparatus, along with details of calibration and data acquisition can be found in Gregory et al. (2018).

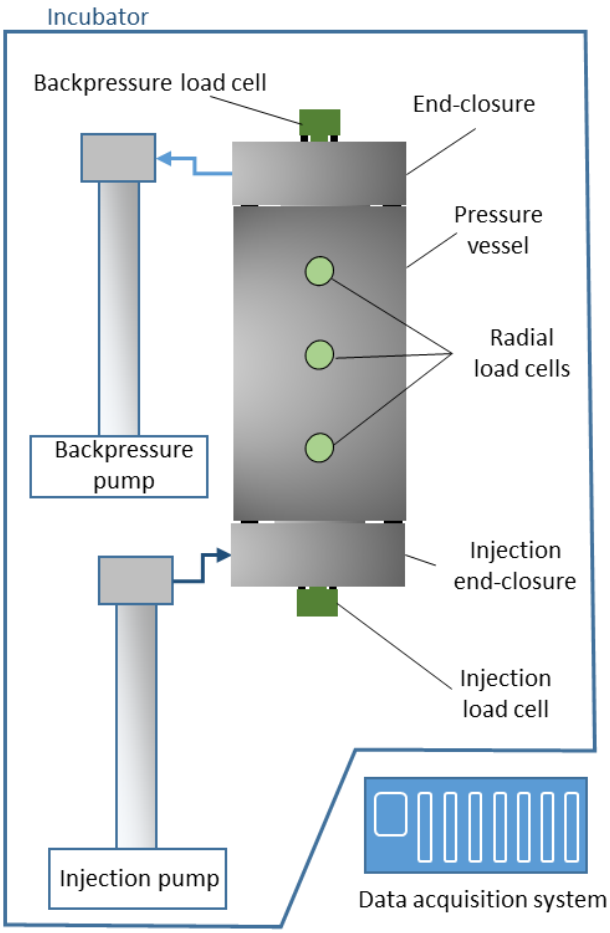

Figure 2 Schematic showing the main components of the CVAF apparatus. The pressure vessel was mounted vertically to avoid gravity effects during flow testing

The MIND-project has received funding from the European Union's Euratom research and training program (Horizon2020) under grant agreement 661880.

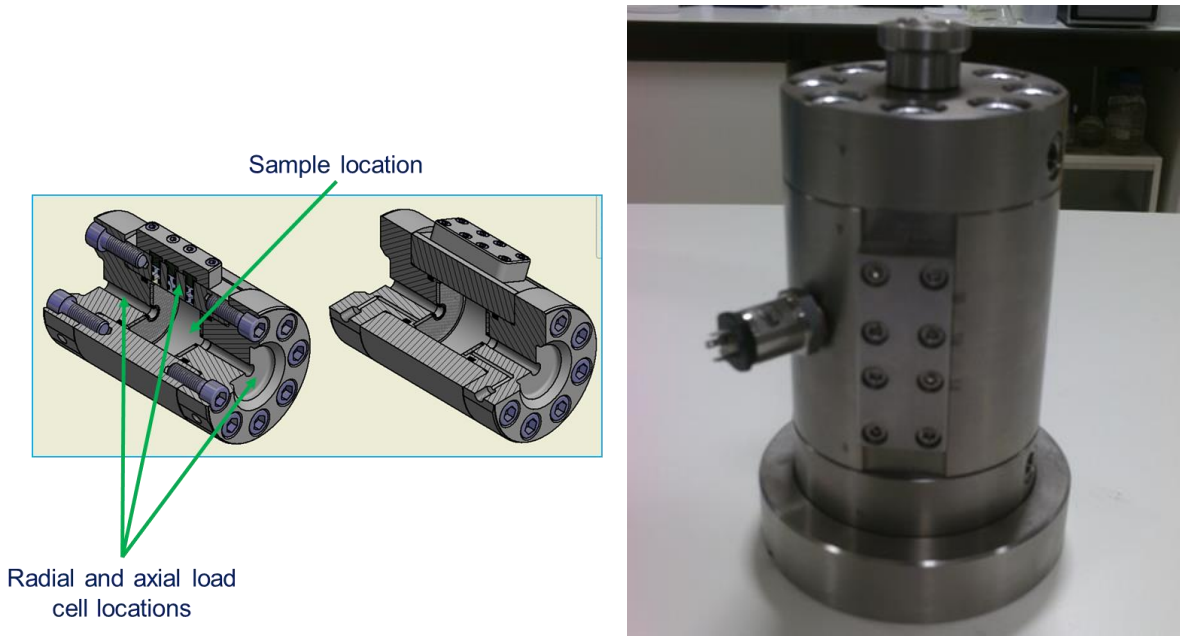

Figure 3 Schematic showing the cut-away section of the CVAF pressure vessel (left) and a photograph of the vessel before plumbing in to the flow system (right).

2.2.2 CVAF conditions

Immediately following preparation and measurement, the sample was sealed into the CVAF vessel which had previously been sterilised with 70% methanol. Following installation of the samples (test stage [0]), equilibration was carried out by applying a nominal pressure of 1.00 MPa to both ends of each specimen to induce swelling of the clay (test stage [1]). The exception to this protocol was BUG023 where a calibration error resulted in an elevated backpressure being applied to the sample (Table 2). Following a swelling period of at least 24 days, a constant pressure test was performed by increasing the injection pressure to 2.50 MPa for the remainder of the experiment (test stage [2]). The injection and back pressure, the pressures at the load cells and the flux in and out of the sample were automatically logged and were monitored throughout each test. Full physical properties, stress and swelling pressure, mineralogical, petrological and microbiological data are presented for samples BUG021 – BUG026. Due to timing of experiments, only data from continuous data monitoring (e.g. swelling pressures and permeability) are presented for BUG027 and BUG028.

The MIND-project has received funding from the European Union's Euratom research and training program (Horizon2020) under grant agreement 661880.

Table 3 Summary of experimental histories showing sample, stage numbers, type of stage (EQ = equilibration, CPT = constant pressure test) and duration of tests

Specimen number [test stage]	Type	Injection pressure (MPa)	Backpressure (MPa)	Length of stage (days)
BUG021 [1]	EQ	1.00	1.05	24
BUG021 [2]	CPT	2.50	1.06	124
BUG022 [1]	EQ	1.01	0.99	24
BUG022 [2]	CPT	2.52	0.99	121
BUG023 [1]	EQ	1.09	1.33	29
BUG023 [2]	CPT	2.48	1.35	122
BUG024 [1]	EQ	1.03	1.00	31
BUG024 [2]	CPT	2.52	1.01	109
BUG025 [1]	EQ	1.01	1.02	37
BUG025 [2]	CPT	2.50	1.02	119
BUG026 [1]	EQ	1.01	1.00	40
BUG026 [2]	CPT	2.50	1.01	118
BUG027 [1]	EQ	1.00	1.06	38
BUG027 [2]	CPT	2.50	1.07	111
BUG028 [1]	EQ	1.01	1.00	32
BUG028 [2]	CPT	2.50	1.02	--

2.2.3 Post experimental sample processing

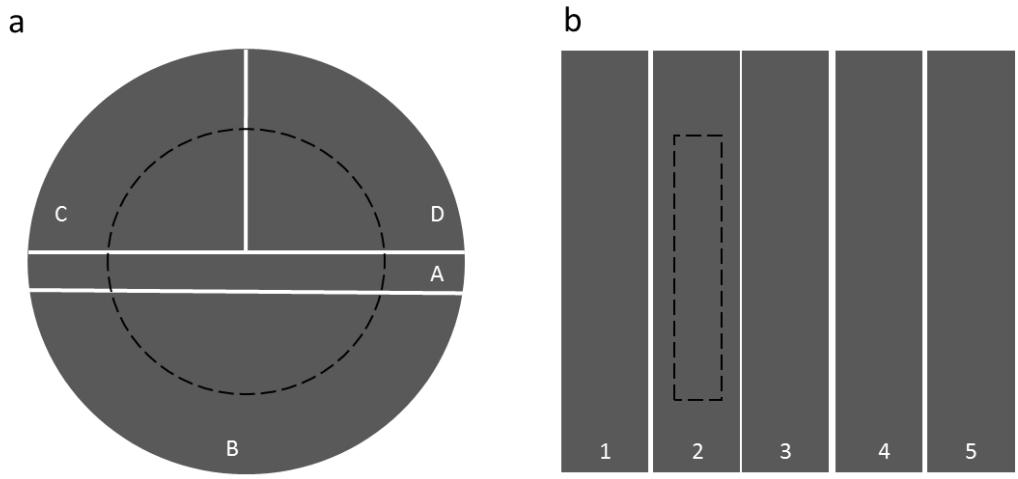

Figure 4 a) Illustration of the longitudinal cuts that were made in the post-experimental sample to allow the division for different analyses: thin sectioning/polished block for SEM and SEM stub analysis (A), microbiological analysis (B), XRD (C) and reference section (D). b) transverse cuts made to the microbiology subsamples (B) (1= inlet end, 5 = outlet end). Dashed line shows approximate extent of steel containing layer in tests BUG021- BUG026. In BUG027 and BUG028 the steel was positioned in the central section of the core so that the corroding steel was adjacent to the axial load cells.

The processing of samples at the end of each experiment and the details of analytical techniques used can be found in (Gregory *et al.*, 2018). Briefly the core sample was divided as shown in Figure 4. Samples of fluids from the injection and backpressure pumps were also collected. Core samples were

The MIND-project has received funding from the European Union's Euratom research and training program (Horizon2020) under grant agreement 661880.

made into a slurry with 0.9% saline solution (1g sample in 6 ml saline). Samples for DNA analysis were frozen at -20^{o}C.

2.3 Analytical methods

2.3.1 SEM analysis

Scanning electron microscopy and X-ray microanalysis

The sub-samples taken for petrographic analysis were analysed as both stub samples and polished thin section or polished blocks. Techniques included scanning electron microscopy (SEM) using both secondary electron imaging and backscattered electron (BSE) imaging and element distribution analysis using digital energy-dispersive X-ray microanalysis (EDXA), elemental mapping and quantitative energy-dispersive electron probe point microanalysis (ED-EPMA). The methodologies used are detailed in Gregory *et al.* (2018)

Low magnification images of the thin sections were recorded by digitally scanning the thin section using an Epson Perfection 1240U flatbed scanner equipped with a transmitted light (transparency) scanning attachment at a resolution of 1200 dpi.

2.3.2 X-ray diffraction

X-ray diffraction (XRD) analysis

XRD analysis of oriented mount samples using an Anton Paar THC (controlled temperature and humidity) was carried out using a PANalytical X'Pert Pro series diffractometer equipped with a cobalt-target tube, X'Celerator detector and operated at 45 kV and 40 mA. The random powder mounts were scanned from 4.5 to 85°2θ at 2.06°2θ min^{-1}. Diffraction data were initially analysed using PANalytical X'Pert HighScore Plus version 4.6 software coupled to the International Centre for Diffraction Data (ICDD, 2018, 2019) database.

2.3.3 Microbiology methods

Most probable number (MPN) counts for SRB, and Miles Misra plate counts for total culturable anaerobic heterotrophs and aerobic heterotrophs were carried out as described previously (Gregory *et al.*, 2018). Analysis was carried out at the end of each test on groundwater collected from the injection and back pressure pumps and on five subsections of the test sample (Figure 4). For BUG021 and BUG022 the MPN method was used for all microbiological enumeration, but difficulties in distinguishing between cloudiness of the media indicating bacterial growth and cloudiness caused by clay in the samples led to a Miles Misra method being adopted for later tests for anaerobic and aerobic heterotrophs.

DNA was extracted from the samples using a FastDNA kit for soils (MP Biomedicals) according to the manufacturer's protocol. Initially 0.5 g sample was used in each extraction. It was noted that the swelling of the bentonite in the first sodium phosphate buffer/MT buffer step of the protocol greatly reduced the effectiveness of the of the bead beating step so various modifications to the protocol were applied, including using slurried sample prepared using a 1:6 ratio of bentonite to sterile 0.9% saline solution, increasing sample volume to 5 g and using a FastDNA 50 ml isolation kit for soil (MP Biomedicals), preparing the bentonite slurry using a phosphate buffer (0.5 M $NaH_2PO_4.H_2O$, 0.5 M Na_2HPO_4 (Högfors-Rönnholm *et al.*, 2018)) to prevent DNA sorption to the bentonite. DNA extracts were eluted in water and stored at –20°C.

qPCR was carried out using PowerUp™ SYBR™ green master mix polymerase (Applied Biosystems™) and the iQ™ Supermix (Bio-Rad®) with 1X SYBR™ gold. Primers targeting the bacterial 16S rRNA gene and the sulphite reductase gene (*dsrA*) were used for the quantification of Bacteria and SRB respectively as described in Table 4.

The MIND-project has received funding from the European Union's Euratom research and training program (Horizon2020) under grant agreement 661880.

Table 4 Quantitative PCR conditions

Target	Primer pair	Initial denaturation (°C / min)	Denaturation (°C,s)	Annealing (°C/s)	Extension (°C/s)	Cycles	Final extension (°C/s)	Reference
16S rRNA (Bacteria)	BAC341F/ BAC534R	95 / 3	98 / 10	63 / 20	72 / 30	35	72 / 120	(Muyzer et al., 1993)
***dsrA* (SRB)**	DSR1F/ RH3R-dsr-R	95 / 2	98 / 10	54 / 15	72 / 30	35	72 / 120	(Ben-Dov et al., 2007)

3 Results

3.1 Swelling pressures and hydraulic properties

3.1.1 Initial swelling pressure in experiments BUG021 – BUG027

Table 5 Initial swelling pressure for samples BUG021 through BUG028. No data is available for BUG028 due a technical problem with the measurement system

Specimen number	Test stage	Mean swelling pressure (MPa)
BUG021	[1]	1.63
BUG022	[1]	2.74
BUG023	[1]	2.76
BUG024	[1]	3.37
BUG025	[1]	0.94
BUG026	[1]	1.18
BUG027	[1]	2.49
BUG028	[1]	--

Following installation of the samples (test stage [0]), a backpressure was applied to both ends of each specimen to induce swelling of the clay in test stage [1] (

The MIND-project has received funding from the European Union's Euratom research and training program (Horizon2020) under grant agreement 661880.

Table 3). *Figure 5* shows the response of tests BUG021 through BUG027 during this phase of the experiment. Data from BUG028 is not shown due to problems with the logging of pressures during this test. While there is some noise in the data (BUG021-BUG027), a transient response is clearly observed in all the tests which then evolves to a series of well-defined asymptotes. Close inspection of the data in BUG023, BUG024 and BUG027, suggest the transient response may have been incomplete by the end of the stage as the stress traces exhibit a small positive gradient. However, estimates of swelling pressure during this phase of testing can be made and are presented in Table 5. As previously reported, inspection of the data suggested that the swelling pressure for BUG021 was significantly lower than that developed in tests BUG022 through BUG024. However, there was some evidence in the data to suggest that samples BUG022 and BUG024 may have been subject to a small 'pre-stress' during the installation phase of each experiment. This has been observed to occur if the cap screws, which retain each end closure, are over-tightened to a higher torque leading to 'stressing' of the sample before hydration and swelling. There was little evidence for significant pre-stressing in sample BUG023 which exhibits a

The MIND-project has received funding from the European Union's Euratom research and training program (Horizon2020) under grant agreement 661880.

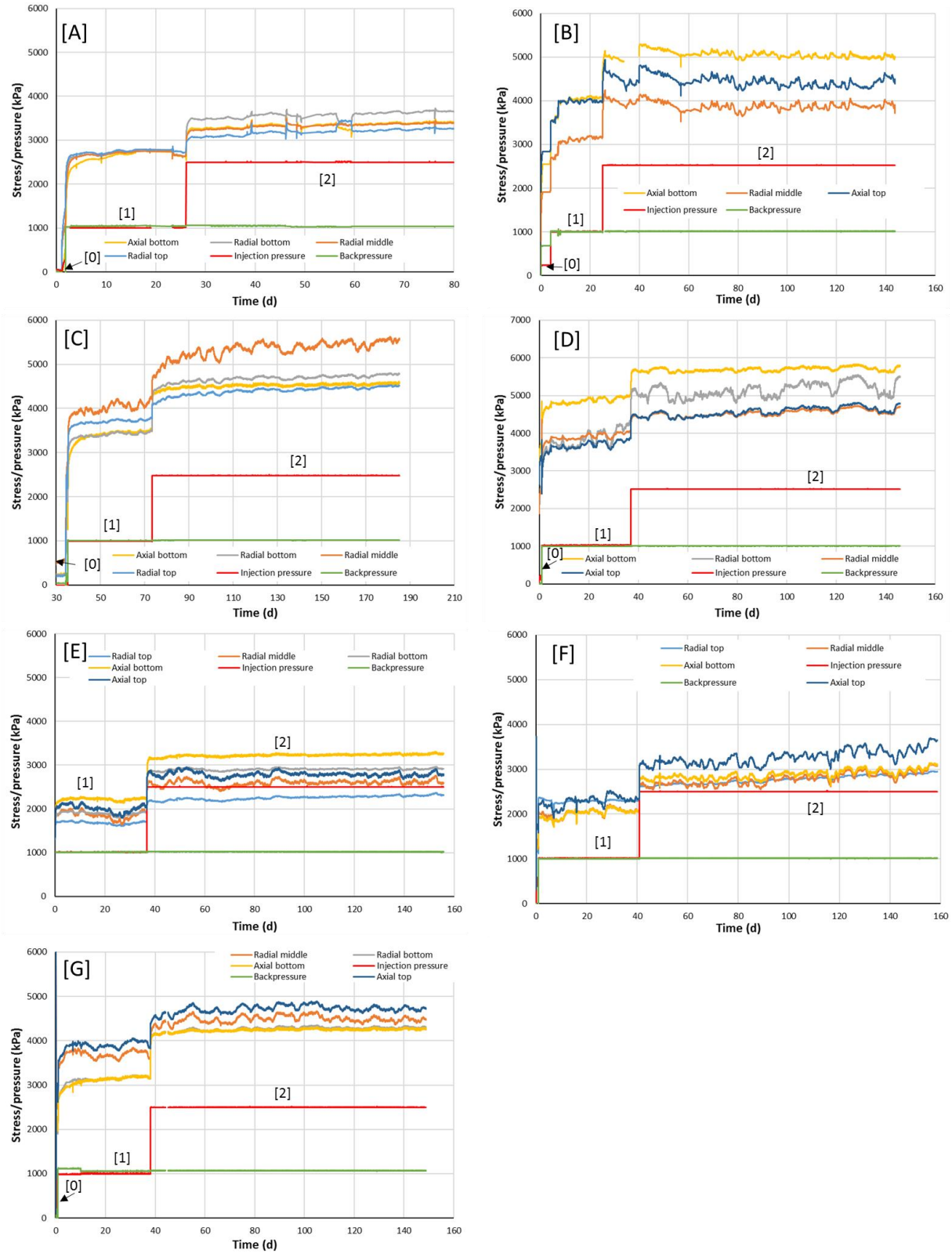

Figure 5 Development of axial and radial stress in tests BUG021 through BUG027 (letters A to G respectively) subject to the boundary conditions presented in Table 3. Numerical values in parentheses denote test stage numbers. Absolute values of stress should be treated with caution due to possible pre-stressing of the samples during installation.

swelling pressure similar to that of BUG022. Comparing the data from Table 5 with estimates for bulk density presented in Table 1, shows a general trend of increasing swelling pressure with increasing

The MIND-project has received funding from the European Union's Euratom research and training program (Horizon2020) under grant agreement 661880.

bulk density. The low swelling pressures observed in BUG025 and BUG026 reflect the lower bulk density of these samples.

3.1.2 Hydraulic properties of the clay

Following the hydration and initial swelling of the samples, a modest hydraulic gradient was applied across each specimen by raising the water pressure in the base (injection) filter to a pre-set value (Table 3). Inflow and outflow data were then measured as a function of time, Figure 6. In test BUG021, Figure 6 [A], only a limited amount of outflow data was available due to problems with the control pump. However, when data became available the values closely matched those of the inflow data, suggesting minimal hydraulic storage and a fully saturated sample. This behaviour was also noted in tests BUG022 and BUG024 through BUG028, Figure 6 [B] and [D] through [H]. However, in test BUG023, Figure 6 [C], outflow evolved more slowly, suggesting a significant period of time was required to reach steady state and thus attain hydraulic equilibrium. The reason for this difference is unclear.

Good mass balance (i.e. minimising the difference between inflow and outflow) was achieved in tests BUG021, BUG022, BUG025 and BUG027. The time-dependent outflow noted above in test BUG023 results in a miss-match between in- and outflow at the end of test stage [2]. Similarly, in test BUG024 a small offset between in and outflow was recorded, indicative of a small leak in either the injection or backpressure systems. This was also the case for BUG026 and BUG028. Careful examination of the data suggests a slight but consistent reduction in inflow/outflow for inoculated samples, Table 5. This is reflected in the average permeability values, which show a similar trend in behaviour.

The application of the hydraulic gradient also resulted in an increase in total stress observed throughout each specimen, *Figure 5* test stage [2]. In all tests, stress rapidly increased following the application of the pressure gradient. This was followed by a period of less rapid stress evolution which slowly evolved into an equilibrium condition. However, in a number of tests, for example *Figure 5*[C], the stress values do not asymptote but continue to slowly increase. This was reflected in the hydraulic data, Figure 6[C], where the development of outflow lagged significantly behind inflow.

However, because the rate of change is very small, it is possible to estimate the swelling pressure of each sample at the end of hydraulic testing to examine what, if any, impact the fluid injection and microbial behaviour had on the mechanical behaviour of the clay (Table 5). In all tests, permeability is seen to decrease in samples which have been inoculated. This is most evident in the lower density tests, BUG025 and BUG026, where microbial activity is likely to be most prevalent. Here permeability is observed to decrease by 20% across the duration of these inoculated test.

The MIND-project has received funding from the European Union's Euratom research and training program (Horizon2020) under grant agreement 661880.

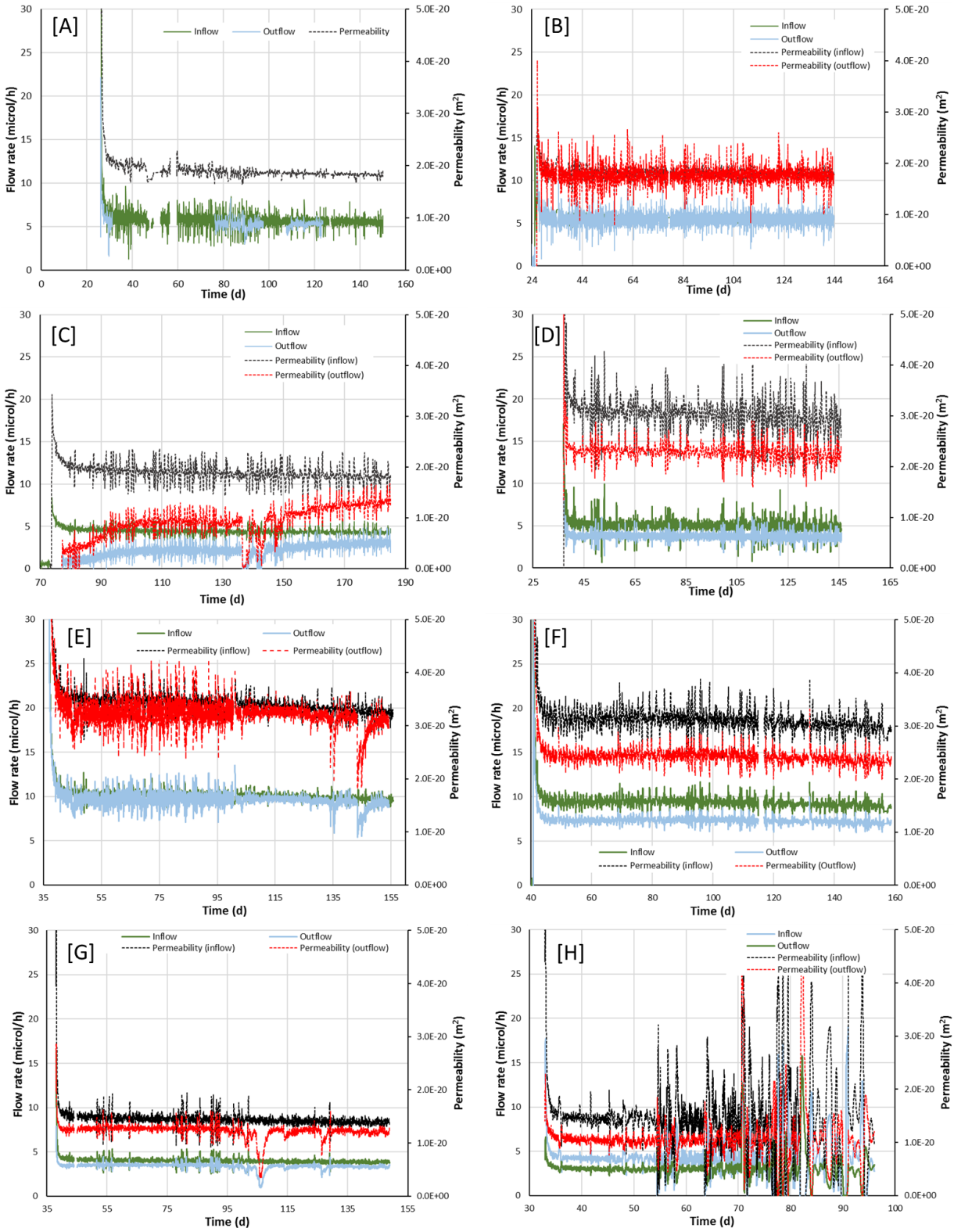

Figure 6 Time averaged hydraulic data from stage [2] of the experiments, showing inflow, outflow and permeability based on the flow data. Letters [A] through [H] denote experiments BUG021 through BUG028 respectively. Flow properties are presented in Table 6

The MIND-project has received funding from the European Union's Euratom research and training program (Horizon2020) under grant agreement 661880.

Table 6 Hydraulic data for samples BUG021 through BUG024

Specimen number	Test stage	Mean inflow (µl h^{-1})	Mean outflow (µl h^{-1})	Permeability - inflow (k) m^2	Permeability - outflow (k) m^2	Mean permeability (k) m^2
BUG021	[2]	5.5	5.2	1.83E-20	-	1.83E-20
BUG022	[2]	5.6	5.5	1.80E-20	1.77E-20	1.78E-20
BUG023	[2]	4.1	3.2	1.49E-20	1.17E-20	1.33E-20
BUG024	[2]	4.8	3.7	1.65E-20	1.26E-20	1.46E-20
BUG025	[2]	10.2	9.7	3.40E-20	3.24E-20	3.32E-20
BUG026	[2]	9.0	7.1	2.99E-20	2.35E-20	2.67E-20
BUG027	[2]	3.8	3.3	1.39E-20	1.20E-20	1.30E-20
BUG028	[2]	4.1	3.0	1.42E-20	1.03E-20	1.22E-20

Table 7 Swelling pressure data for samples BUG021 through BUG028 before (stage [1], Table 3) and after (end of stage [2]) flow testing. No data for BUG028 was available due to problems with the measurement system.

Specimen number	Test stage	Initial swelling pressure (MPa)	Final welling pressure (MPa)	Difference in swelling pressure (MPa)
BUG021	[2]	1.63	1.66	-0.03
BUG022	[2]	2.74	2.65	-0.09
BUG023	[2]	2.76	3.10	0.38
BUG024	[2]	3.37	3.45	0.08
BUG025	[2]	0.94	1.02	0.08
BUG026	[2]	1.18	1.44	0.26
BUG027	[2]	2.49	2.66	0.16
BUG028	[2]	--	--	--

The MIND-project has received funding from the European Union's Euratom research and training program (Horizon2020) under grant agreement 661880.

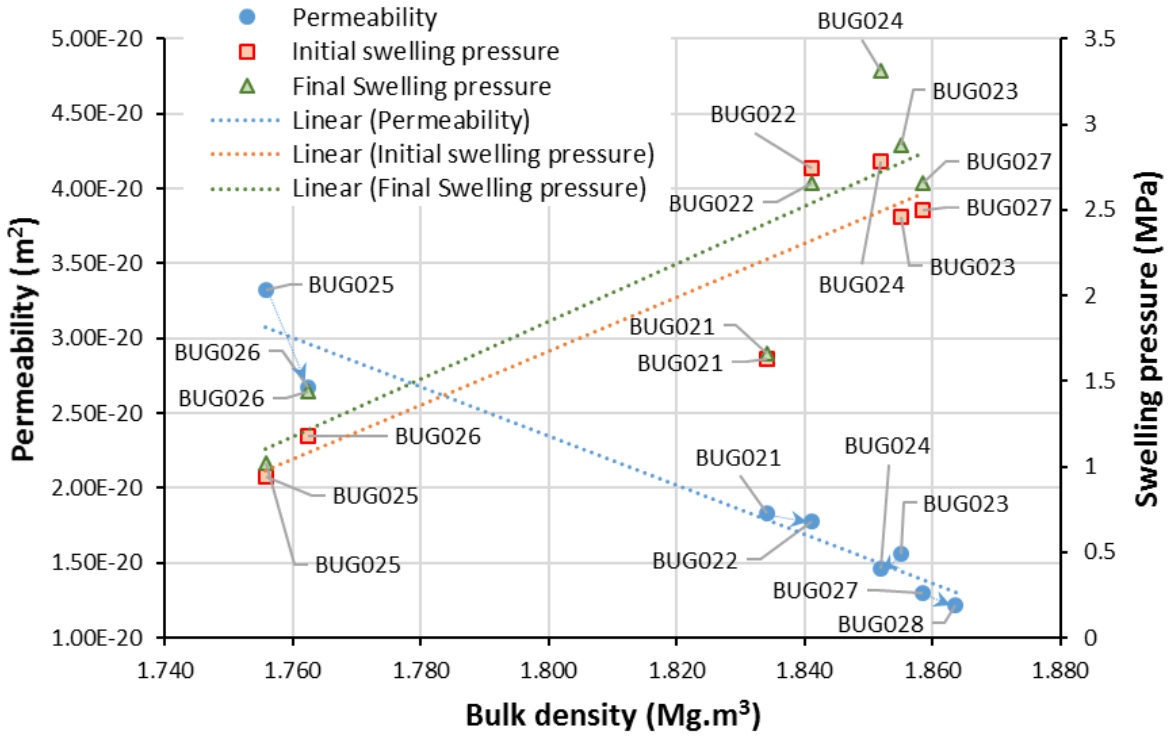

Figure 7 Summary plot showing permeability and swelling pressure (prior to and at the end of hydraulic testing) plotted against estimated bulk density. Trend lines have been added to graph to help identify underlying behaviour.

3.2 SEM analysis

3.2.1 Summary of data from report D2.9 (Gregory et al., 2018)

BUG021 (1400 kg m^{-3} dry density, sterile, no lactate)

No sub-sample for stub analysis was taken from BUG021 due to the limited distribution of the steel filings within the bentonite plug. Noticeable alteration was visible in the polished thin section within the bentonite around the iron filings. This sample showed evidence of microfractures forming during the experiment, not solely as a result of post experiment dehydration. Microfractures were lined and enriched with iron which could only have occurred if the microfractures were open during the experiment. A full description of this sample, with images can be found in (Gregory *et al.*, 2018).

BUG022 (1400 kg m^{-3} dry density, inoculated, no lactate)

This experiment was sub-sampled for stub secondary electron characterisation as well as for polished block analysis. A discolouration of the stub sample was noted with a dark brown colouration of the bentonite around the steel filings surrounded by an orange brown colouration halo penetrating approximately 2 mm further into the bentonite. Acicular aragonite was noted growing into open pore space in fractures, as well as a fibrous iron-rich phase and a silica-rich coating around some grains. A full description of this sample, with images can be found in (Gregory *et al.*, 2018).

BUG023 (1400 kg m^{-3} sterile, lactate added)

This sample was sub-sampled for SEM characterisation by secondary electron imaging. Previously, only analysis of a stub sample was carried out. Little alteration or secondary phases were noted from the secondary electron imaging. A full description of this stub sample, with images can be found in (Gregory *et al.*, 2018).

The MIND-project has received funding from the European Union's Euratom research and training program (Horizon2020) under grant agreement 661880.

BUG024 (1400 kg m^{-3} dry density inoculated, lactate added)

The stub sub-sample showed extensive precipitation of secondary phases including acicular aragonite and a fibrous Fe-phase which appeared to have precipitated over the aragonite layer. A full description of this stub sample, with images can be found in (Gregory *et al.*, 2018).

3.2.2 SEM analysis- Full description of new data

BUG023 (1400 kg m^{-3} sterile, lactate added)

Observation of polished blocks of the BUG023 sample showed that there was very little brown / yellow ferruginous staining around the iron filings within the sub-sample immediately after removal from the experimental rig (Figure 8), but following vacuum drying of the sample, a strong brown staining was visible (Figure 9).

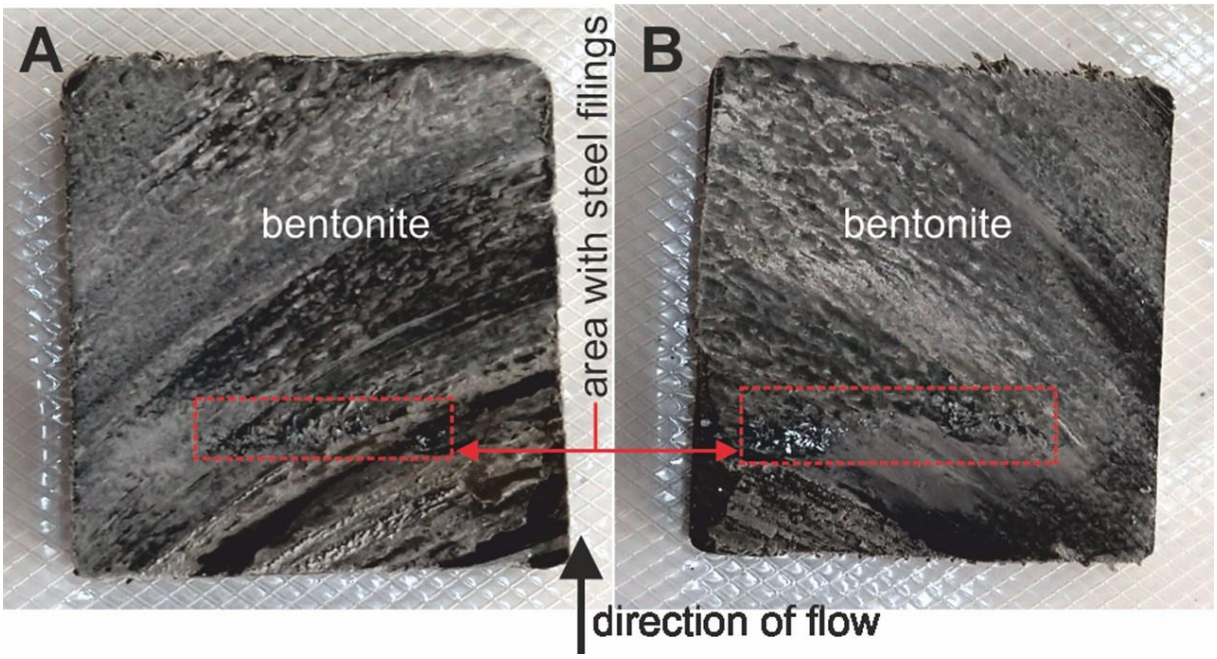

Figure 8 A and B) The first cut of the sample following removal of BUG023 from the anoxic CVAF vessel. Note that there is little staining around the steel filings

The MIND-project has received funding from the European Union's Euratom research and training program (Horizon2020) under grant agreement 661880.

Figure 9 . A and B) The stub section following SEM analysis and exposure to air, showing strong brown staining

The polished block revealed more alteration than in the stub sub-sample, but it was still limited compared to observations from the other samples. Some secondary calcium carbonate including rare aragonite needles was present, together with some Fe-enrichment within the bentonite around the steel filings (Figure 10). Elemental mapping clearly indicates some Ca-enrichment occurring immediately adjacent to a steel filing (Figure 11). Of all the samples examined, this was the most limited in terms of observed alteration and precipitation of secondary phases.

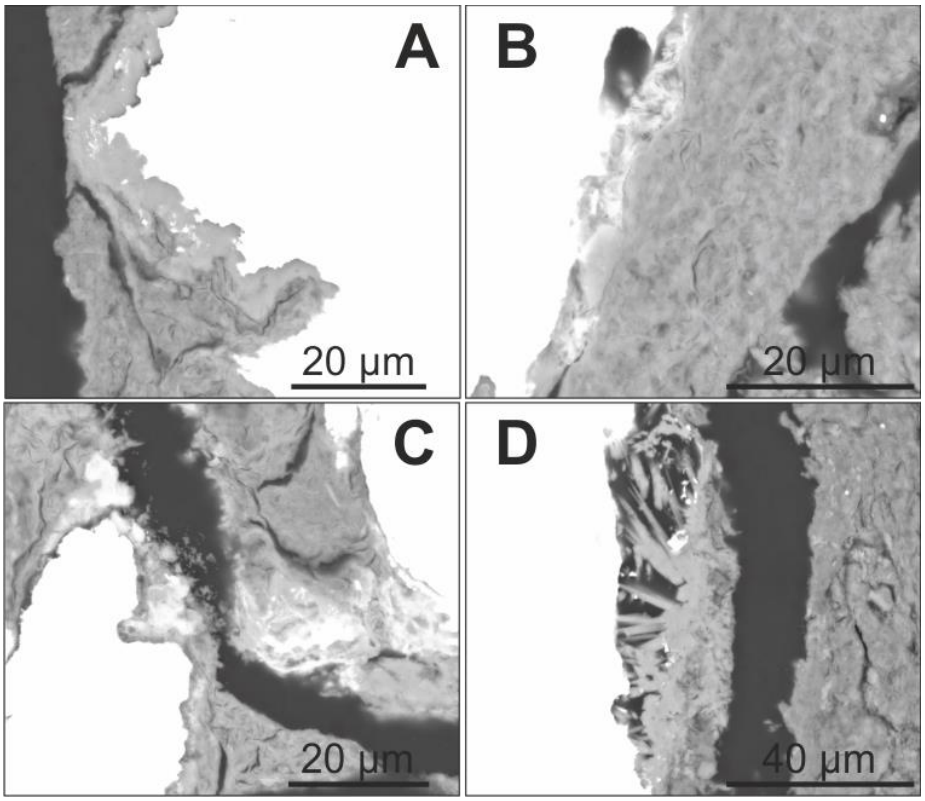

Figure 10. SEM images of BUG023 polished block showing some alteration around the iron filings. Some calcium carbonate (A and D, including aragonite needles (D)) is present, as well as some Fe enhancement (B and C).

The MIND-project has received funding from the European Union's Euratom research and training program (Horizon2020) under grant agreement 661880.

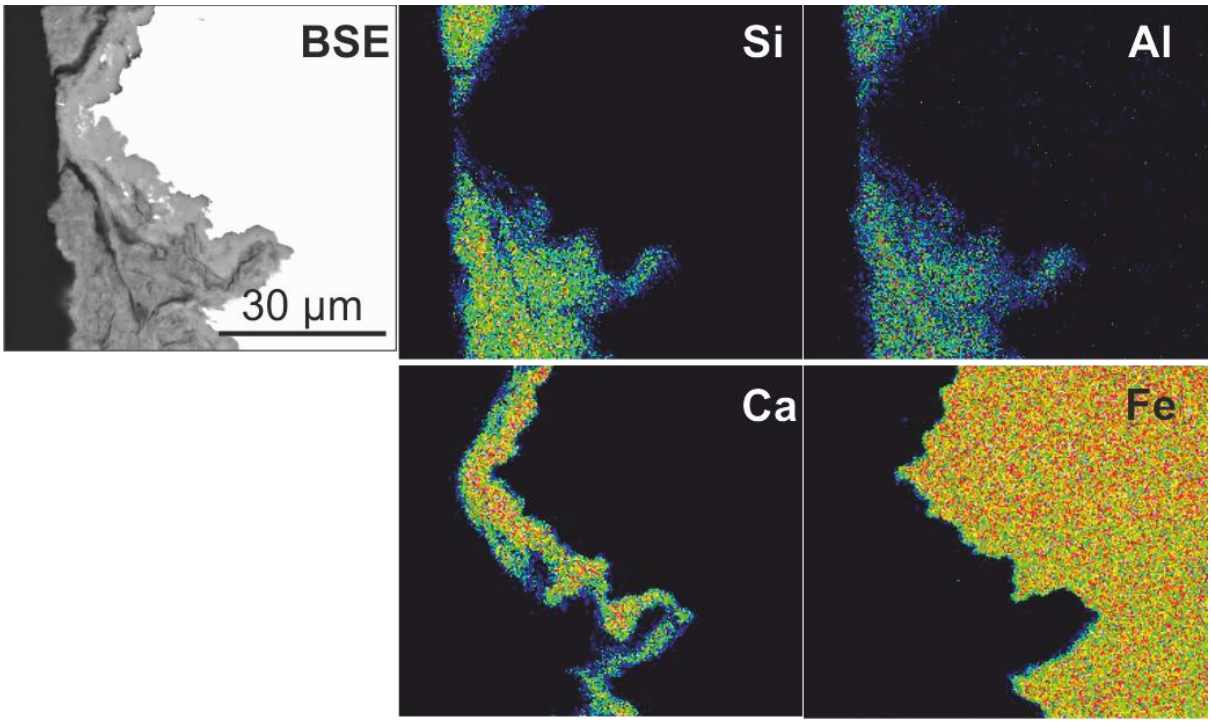

Figure 11. BSEM image and corresponding EDXA microchemical maps of the same area for BUG023 polished block, showing Ca enhancement around the iron filing. Colour concentration scale: red=high concentration, blue/black =low concentration.

BUG024 (1400 kg m^{-3} dry density inoculated, lactate added)

There was a noticeable greenish tinge around the steel filings when initially removed from the CVAF vessel and cut open (Figure 12). However, when the samples were removed from the vacuum bags for further analysis, there were noticeable brown halos around the steel filings, again suggesting the presence of 'green rust'.

SEM images from the polished block confirmed the presence of the fibrous Fe-material and the acicular aragonite noted from the stub sub-sample. However, the polished blocks clearly show the fibrous iron phase has precipitated around the iron filing and the aragonite has precipitated over this layer (Figure 13). The elemental maps clearly show the fibrous iron is an oxidised phase (Figure 14).

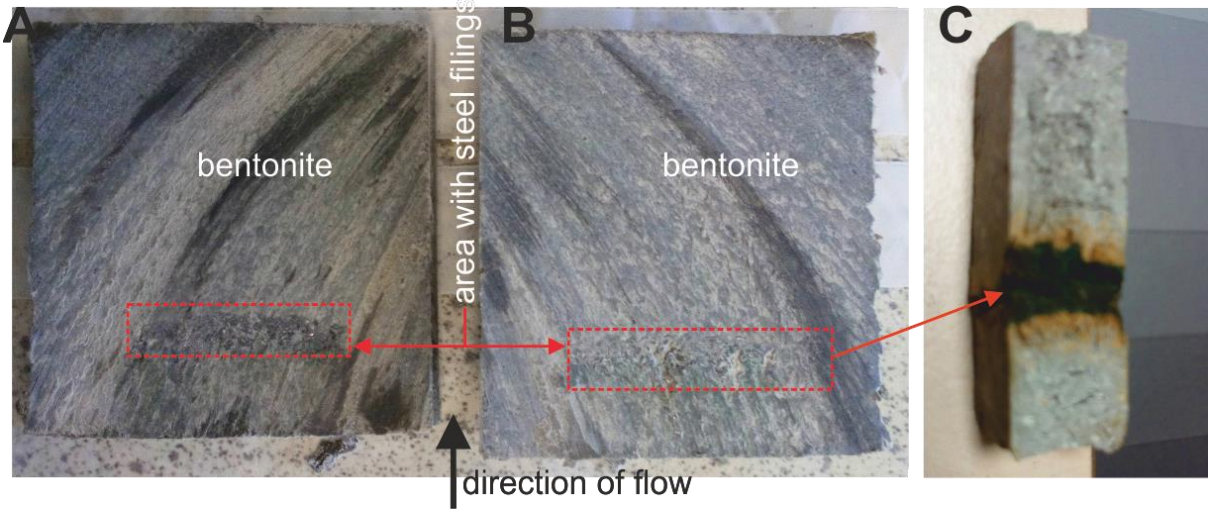

Figure 12 A and B) The first cut of the sample following removal of BUG024 from the anoxic CVAF vessel. Note that steel filings are barely discernible. C) The stub section following SEM analysis and exposure to air, showing the blackening around the steel filings, and ochre colouration into the bentonite.

The MIND-project has received funding from the European Union's Euratom research and training program (Horizon2020) under grant agreement 661880.

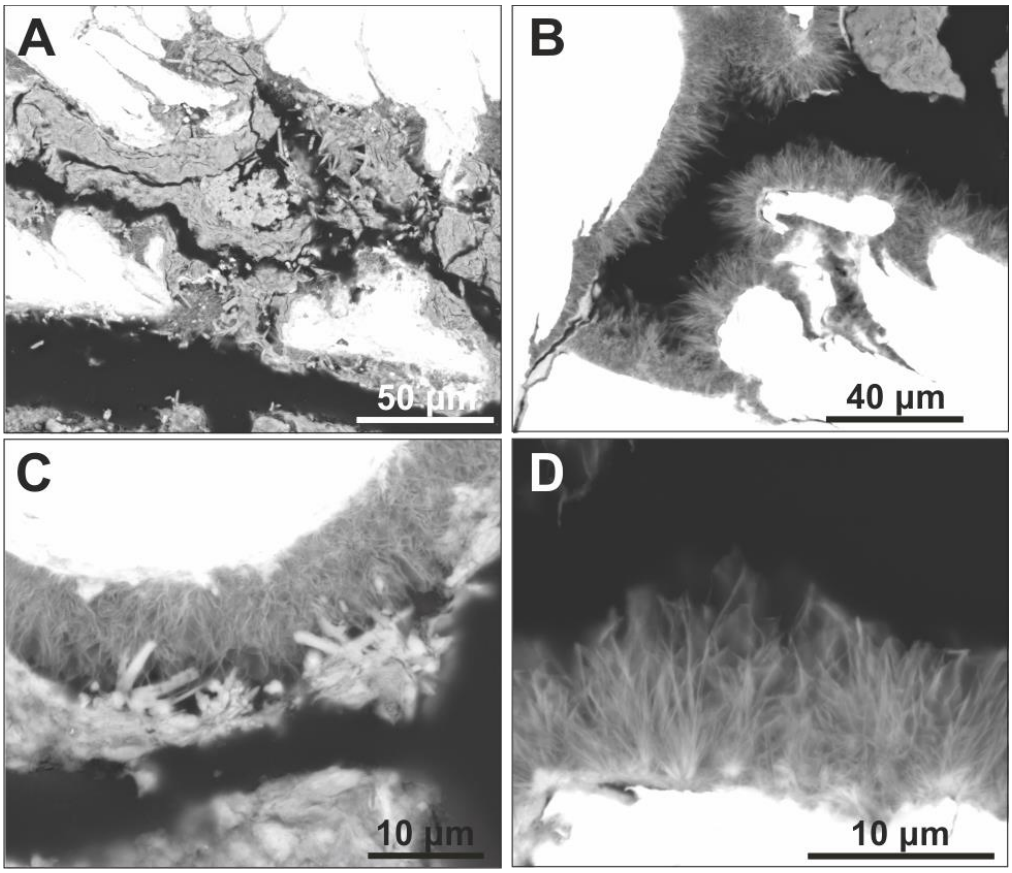

Figure 13 BSEM images from the polished block of sample 24. The layer of fibrous iron is clearly visible surrounding the iron filing. Acicular aragonite is seen precipitating over this layer. A) A low magnification view showing the distribution of aragonite and fibrous Fe phase. B) Fibrous iron infilling open fracture space. C) Aragonite precipitating over the fibrous iron. D) High magnification image of the fibrous iron.

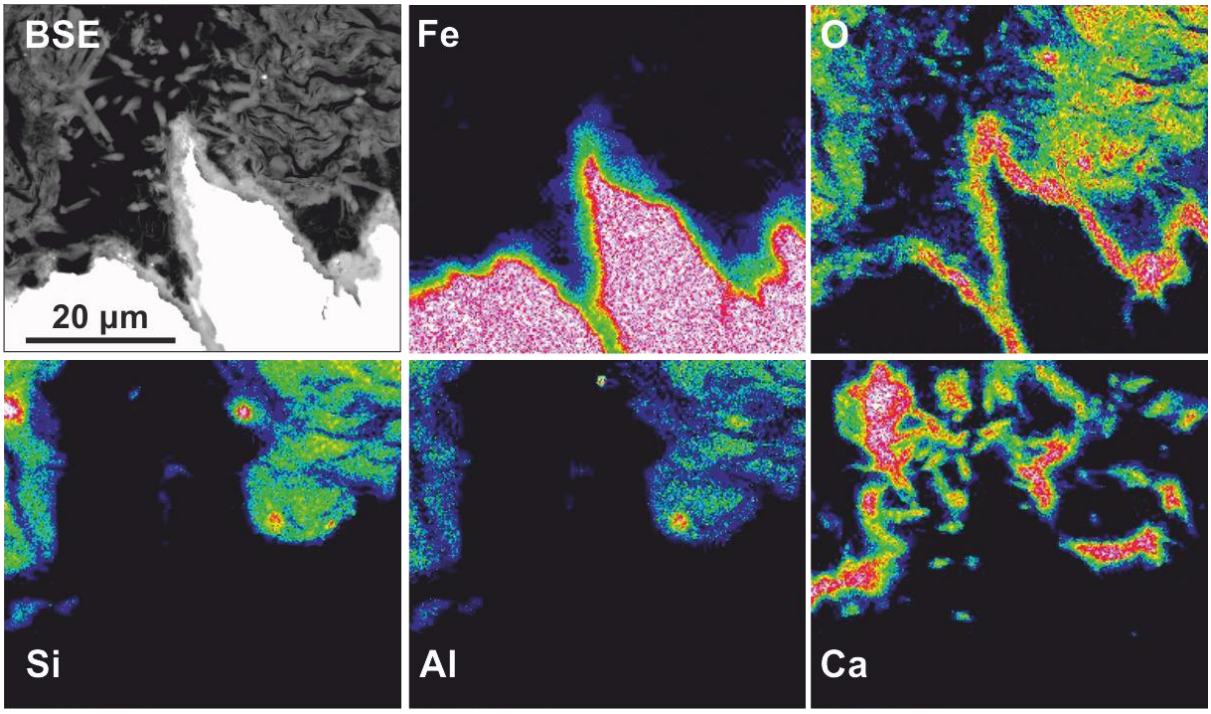

Figure 14. BSEM image and corresponding EDXA microchemical maps of the same area for Fe, O, Si, Al and Ca of an area of iron filings and bentonite from BUG 024. The fibrous iron is an oxidised iron phase, clearly shown by the Fe and O maps. The calcium phase (acicular aragonite) is infilling the pore space. Colour concentration scale: red=high concentration, blue/black =low concentration

The MIND-project has received funding from the European Union's Euratom research and training program (Horizon2020) under grant agreement 661880.

BUG025 (1200 kg m^{-3} dry density, sterile, lactate added)

There was a noticeable greenish tinge around the steel filings when initially removed from the experimental capsule and cut open (Figure 15 and Figure 19). As with previous samples, when the samples were removed from vacuum packing for further analysis, there was a noticeable brown halo around the steel filings, again suggesting the presence of 'green rust'.

The stubs show a proliferation of secondary phases coating the surfaces forming dense mats. Fe-rich phases with a variety of morphologies (fibrous, platy, and globular) together with acicular aragonite are present (Figure 16). This is the first sample which has had fine-grained Fe phases visible within and on the bentonite away from the Fe-filings (Figure 17).
The polished block provides further insight into the extent of the precipitation of the secondary phases and the interaction of the iron and calcite phases within this sample (Figure 18). This is complex, as illustrated by the elemental map which shows that Fe-oxide phases as well as fibrous Fe-S phases are present (Figure 19). A globular Fe-oxide phase is also coated by calcium rich material (including aragonite).

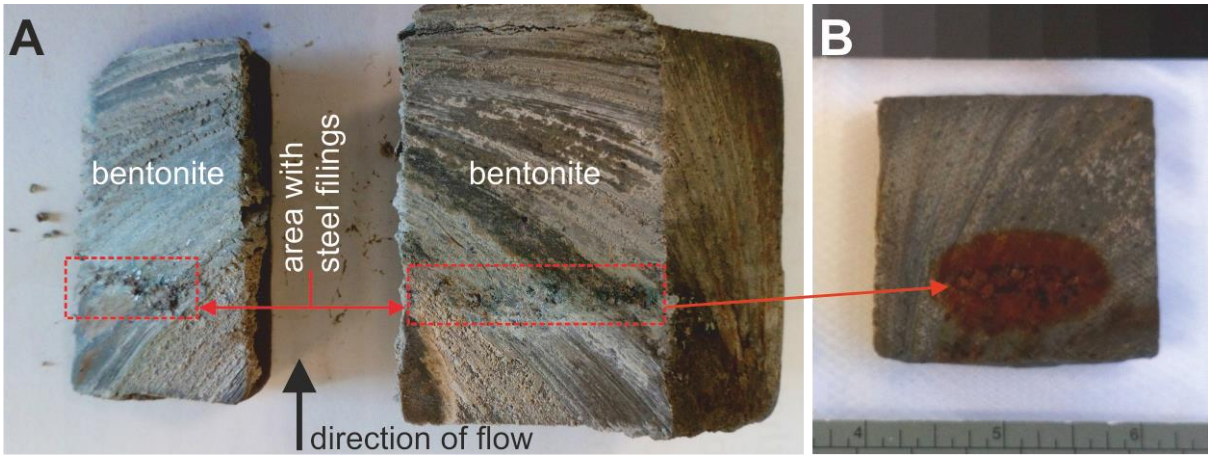

Figure 15 A) BUG025 sample immediately after removal from the experimental capsule and initial cutting – note the green colouration around the steel filings (green rust?). B) Immediately after removal from the vacuum pack prior to vacuum drying. Note the change in colouration and the obvious ochre halo around the filings. Exposure to air during the initial cutting prior to vacuum packing within gas tight vacuum bags was sufficient to oxidise the material.

The MIND-project has received funding from the European Union's Euratom research and training program (Horizon2020) under grant agreement 661880.

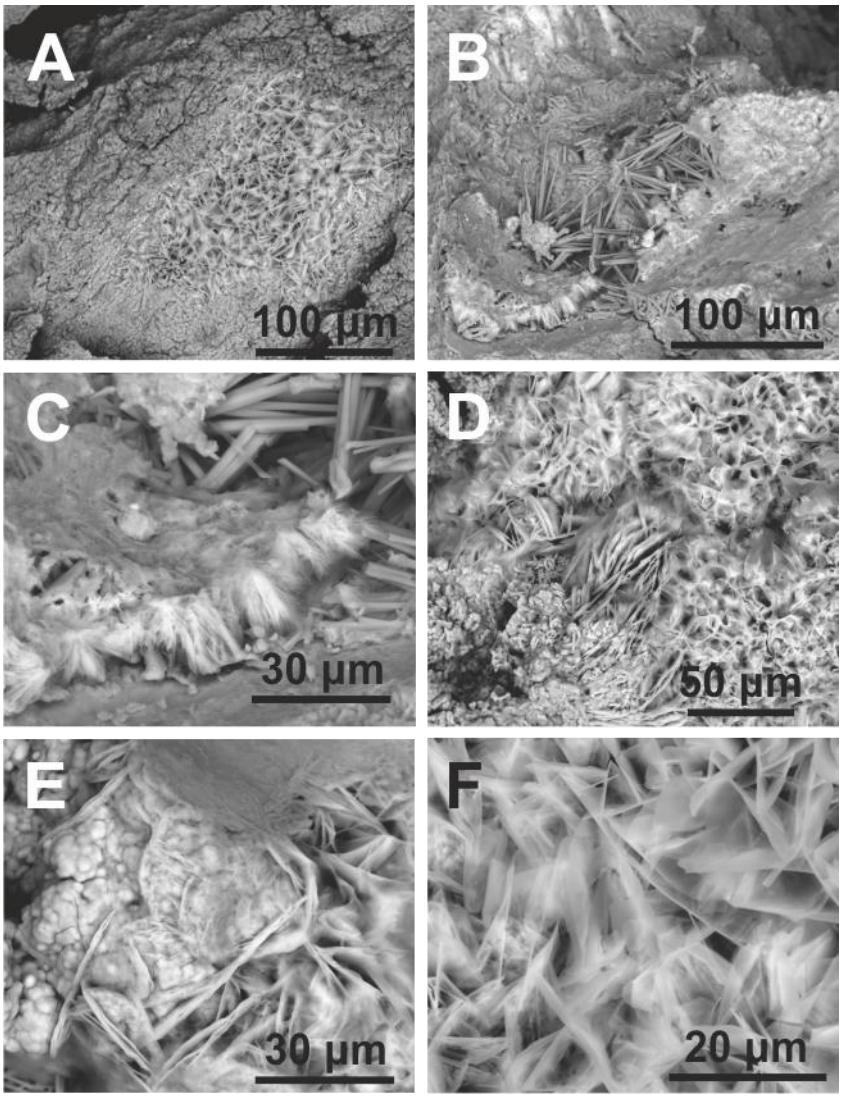

Figure 16, BSE images of sample BUG025 stub showing a proliferation of secondary phases. A and B) Lower magnification images showing the carpeting of the bentonite and steel filings in fibrous and acicular phases. C) This image shows the thin layer of fibrous iron coating the underlying material. Top right of the image is acicular aragonite. D) A variety of morphologies of Fe-rich material. E and F) Higher magnification images showing detail of the morphologies.

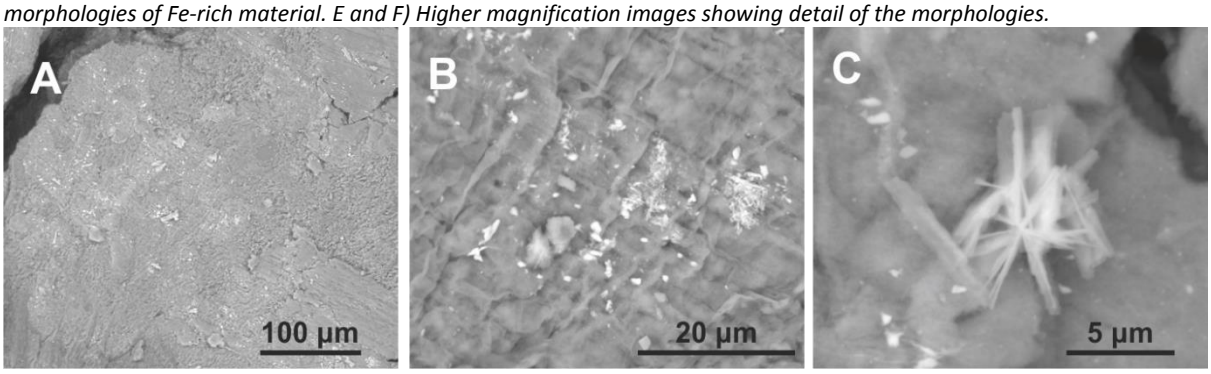

Figure 17. BSE images of sample BUG025 stub showing Fe secondary phases on and within the bentonite. This is the first sample in which fine grained iron precipitation has been observed within the bentonite away from the Fe-filings. A-C increasing magnification.

The MIND-project has received funding from the European Union's Euratom research and training program (Horizon2020) under grant agreement 661880.

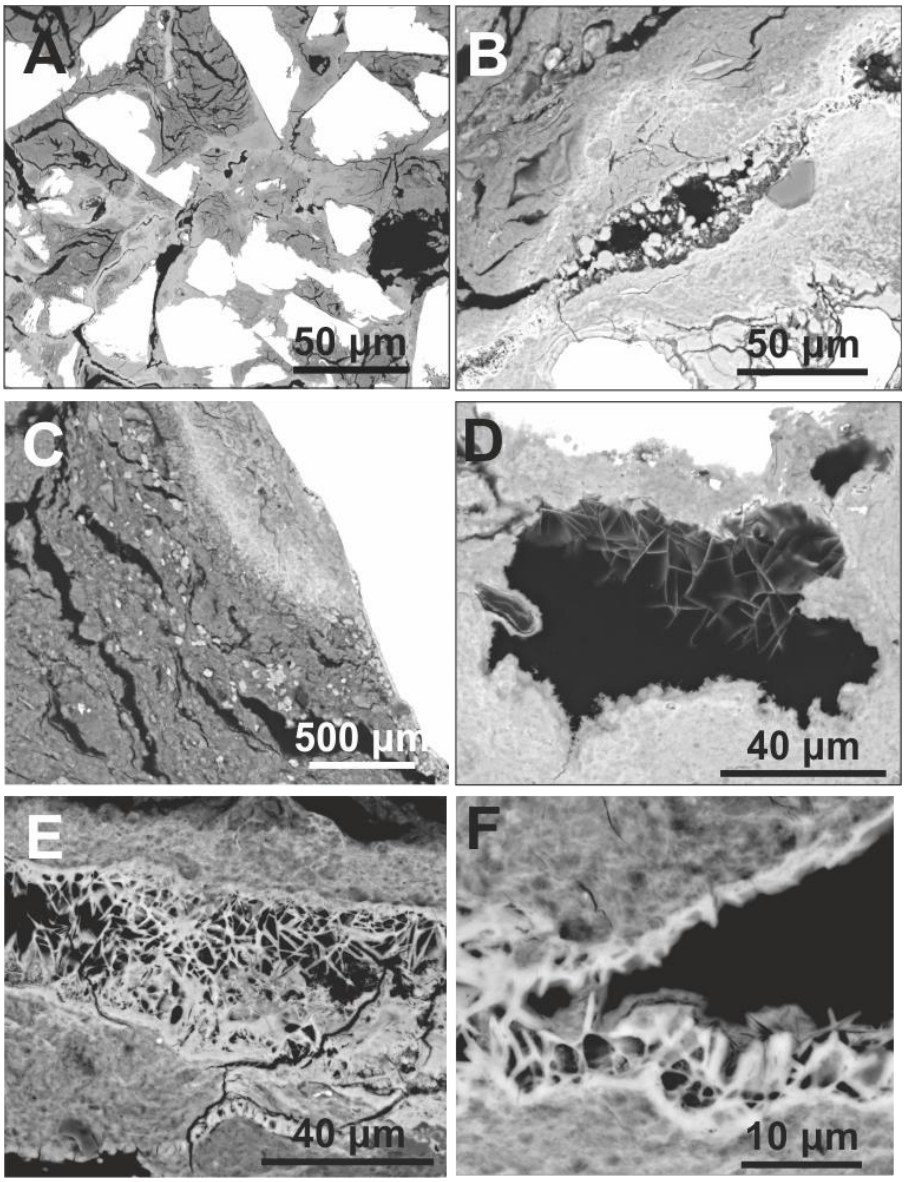

Figure 18. BSE images of the polished block for sample BUG025. A) Low magnification view showing the extent of iron enrichment around the iron filings. B) Fe enrichment within the bentonite and precipitation, and aragonite within a fracture space around the iron filings. C) Iron and calcium enrichment and secondary phases within the bentonite. D-F) Fibrous Fe-rich and calcium-rich phases.

The MIND-project has received funding from the European Union's Euratom research and training program (Horizon2020) under grant agreement 661880.

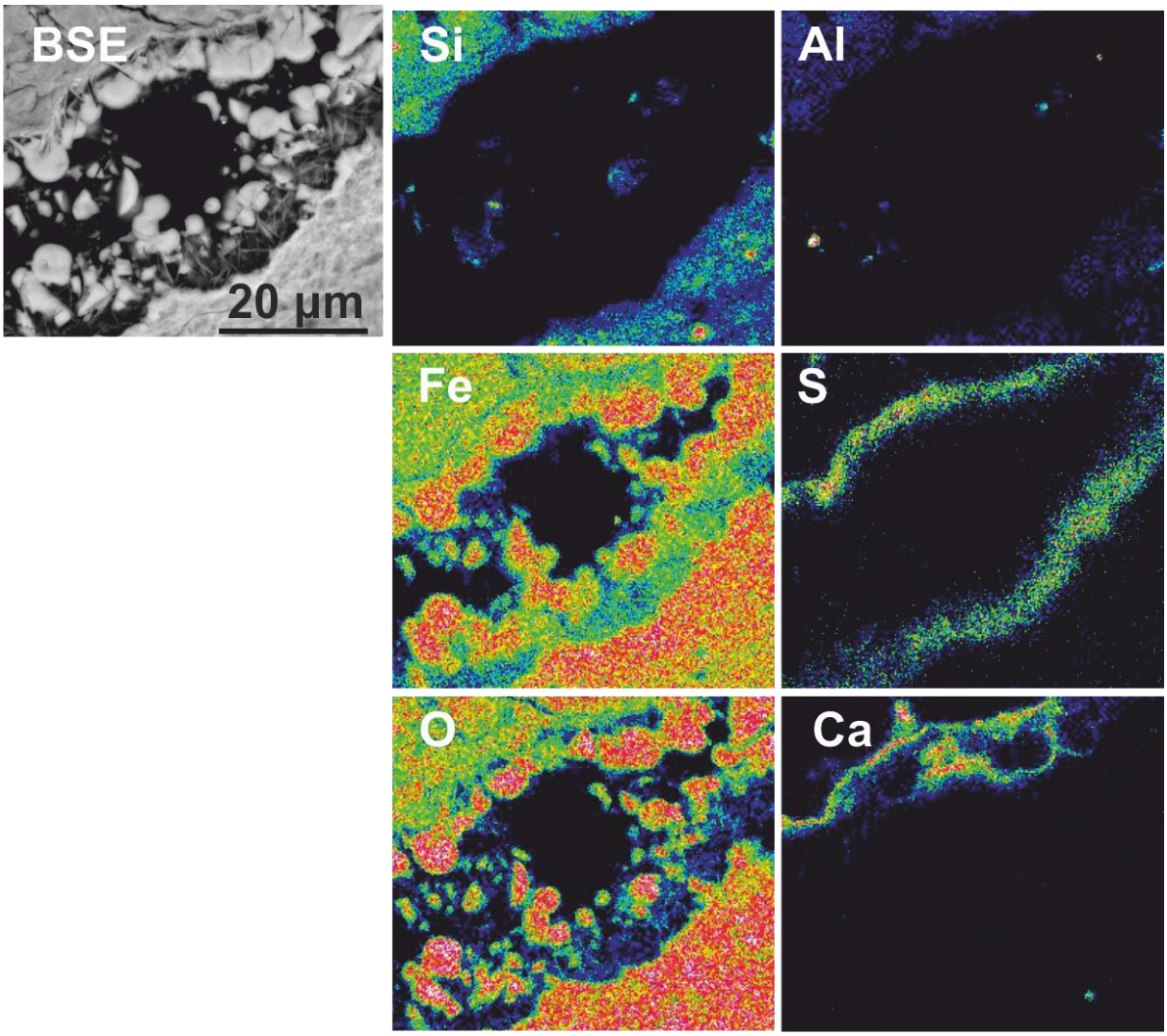

Figure 19. BSE image and corresponding EDXA microchemical maps of the same area for Si, Al, Ca, Fe and S. The iron filing is located approximately 60 microns further from the bottom right of this field of view. The secondary precipitation is complex here. The bentonite (bottom right and top left) have been coated (or replaced) with an iron oxide phase. At the interface with the bentonite and the void, a layer of Fe-S fibrous material is present. At the uppermost interface, calcium enrichment is also present and this has also precipitated around a globular, Fe-oxide phase. Colour concentration scale: red=high concentration, blue/black =low concentration

BUG026 (1200 kg m^{-3} dry density, lactate added, inoculated)

There was a slight greenish tinge around the steel filings when initially removed from the experimental capsule and cut open, although this was not as pronounced as in BUG025. On removal from vacuum packed bags, the samples had noticeable brown halos around the steel filings suggesting the presence of 'green rust' which can rapidly oxidise if exposed to air.

Observations on the stub sub-sample revealed occasional acicular aragonite crystals. These appeared 'flat' compared to the radial nature of previous samples – this is possibly due to the available pore space within the fracture being very limited (Figure 21), although Figure 7 suggests that this sample has some of the highest permeability of all the samples. Amongst the acicular aragonite, small (< 1 µm), Fe-rich particles were present. On the bentonite surface (Figure 22), tight clusters comprising thin plates of Fe-rich material form 'polka-dots' (up to 500 µm).

The MIND-project has received funding from the European Union's Euratom research and training program (Horizon2020) under grant agreement 661880.

The polished block confirmed the presence of calcium carbonate, some of which was acicular aragonite (Figure 23C). Very fine fringes of Fe material at the interface of the steel filings and the bentonite was present in places (Figure 23D). Elemental mapping suggests this is an oxidised Fe phase. No sulphur was detected.

The filings themselves appear to be particularly embayed in this sample with the embayed areas often comprising of void space. This may be due to the corrosion consuming the water but secondary phases not yet having precipitated.

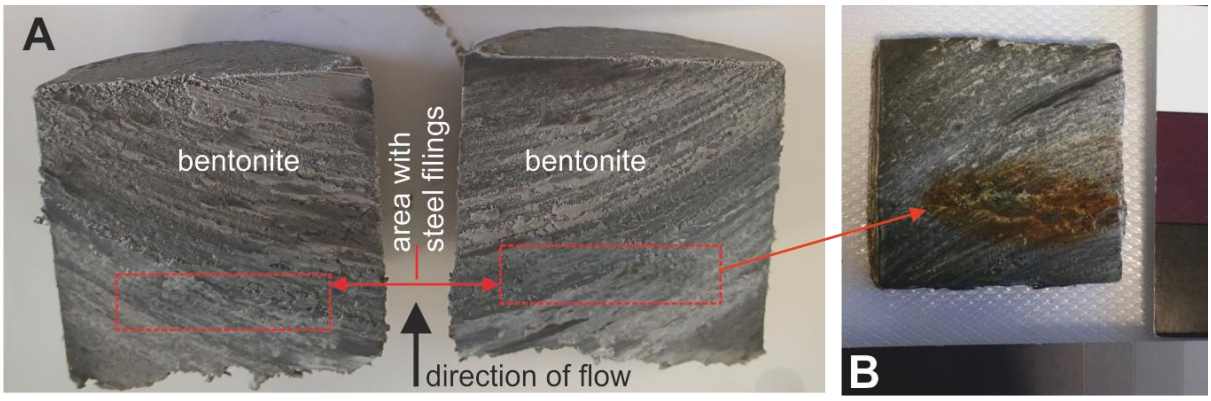

Figure 20 A) BUG026 sample immediately after removal from the experimental capsule and initial cutting – there is a slight green colouration around the steel filings, but this is less pronounced than in BUG025. B) Immediately after removal from the vacuum pack prior to vacuum drying. Note the change in colouration and the obvious ochre halo around the filings. Exposure to air during the initial cutting prior to vacuum packing within gas tight vacuum bags was sufficient to oxidise the material.

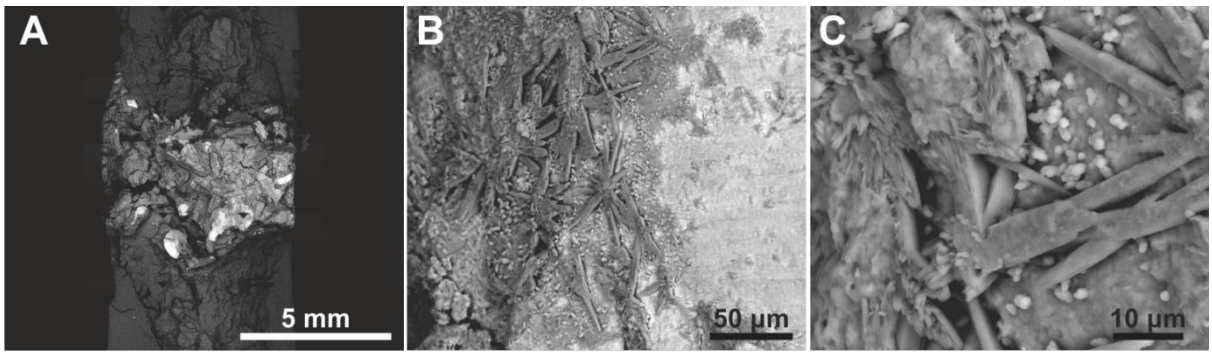

Figure 21. A) BSE photomontage of the central area of the stub section showing the extent of the Fe enrichment around the Fe-filings. B and C) BSE images of acicular aragonite. This was sparse, and had a flattened appearance suggesting the void space was narrow, and the acicular needles precipitated along the fracture. EDXA point analysis indicates the fine light-coloured particles are Fe-rich.

The MIND-project has received funding from the European Union's Euratom research and training program (Horizon2020) under grant agreement 661880.

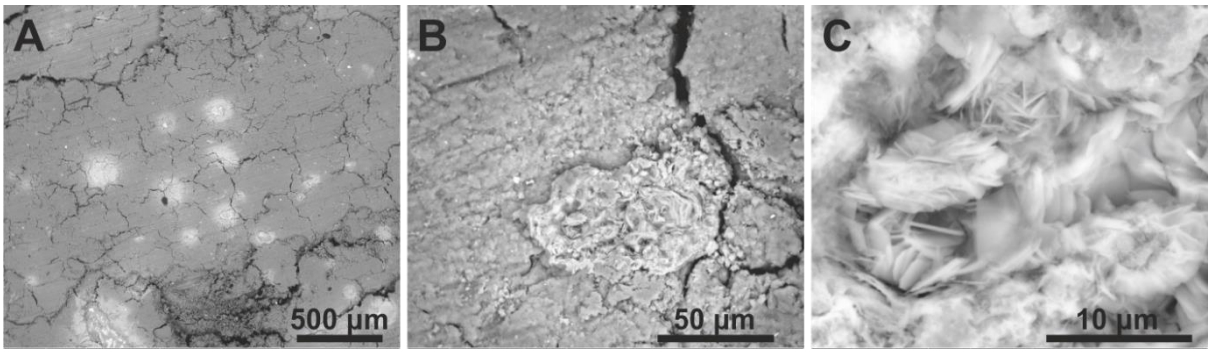

Figure 22. BSEM images of Fe-rich 'polka-dot' phases on the surface of the bentonite. These have a fibrous / platy morphology.

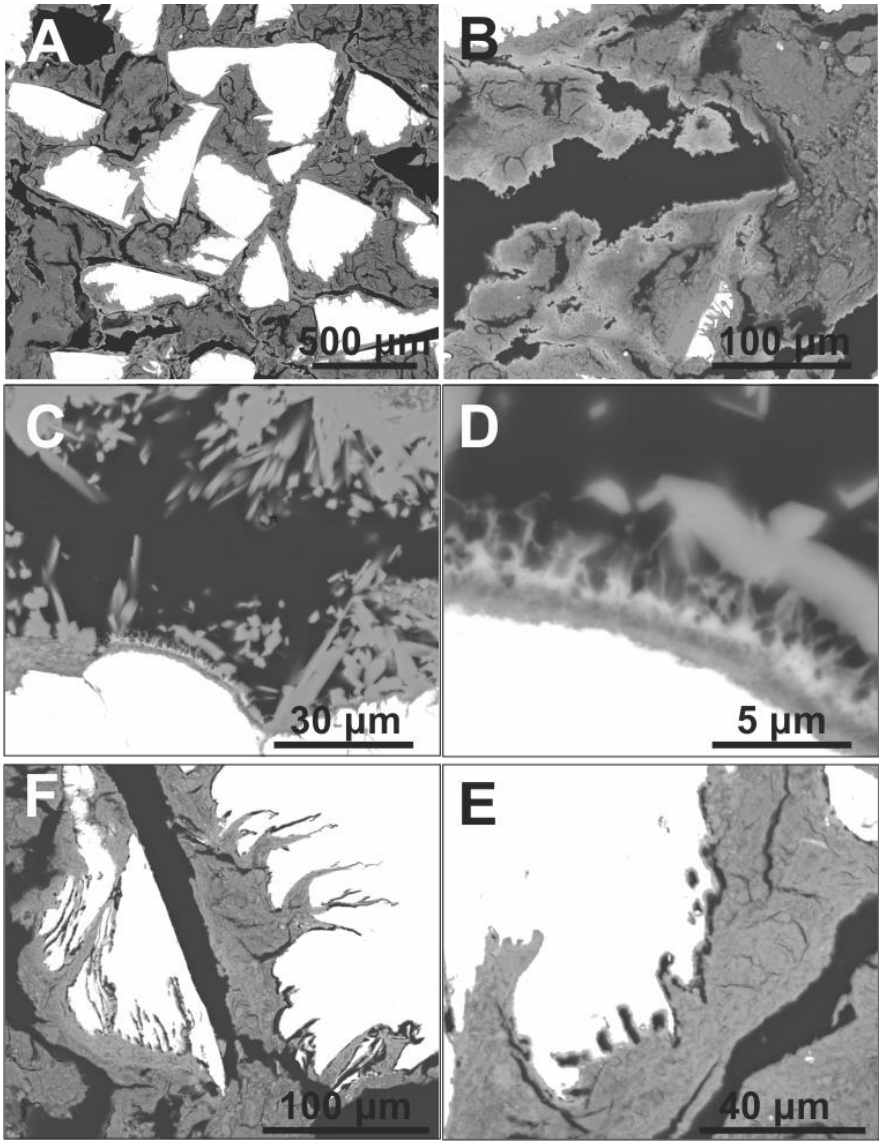

Figure 23. BUG026: BSE images from the polished block. A) Low magnification image – less secondary iron enrichment is visible than BUG025. B) Iron enrichment within the bentonite. C) Rare acicular aragonite. D) High magnification image of C showing an iron-rich fringe around an iron filing. F and E) the iron filings in this sample appeared to be far more embayed than in previous samples, very often with no secondary infill i.e. filled with void space.

The MIND-project has received funding from the European Union's Euratom research and training program (Horizon2020) under grant agreement 661880.

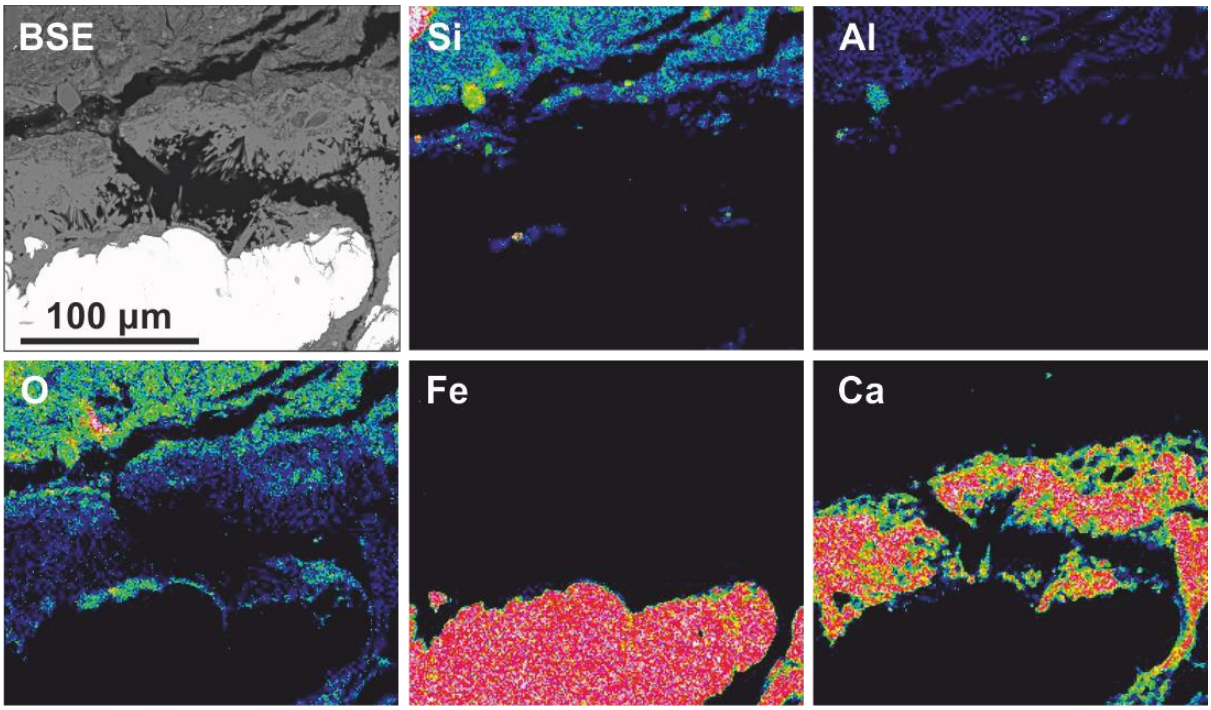

Figure 24 BSE image and corresponding EDXA microchemical maps of the same area for Si, Al, O, Fe and Ca. Sample BUG026.Extensive secondary calcium carbonate within void space, including acicular aragonite. Thin fringe of oxidised Fe around the iron filing. No S was detected. Colour concentration scale: red=high concentration, blue/black =low concentration

3.2.3 Petrology summary

The results of the petrological analysis show a wide variation in the types of secondary precipitation (e.g. morphologies) and volume of material. Calcium carbonate and iron oxide phases dominated with Fe-sulphide only present in BUG025. A green tinge was noted in samples from tests BUG023 – BUG026, which rapidly changed to brown halo on exposure to air. Although this was not noted in earlier samples it may have been overlooked as the green tinge rapidly disappeared. Unfortunately, as the green colour is transient, it is not possible to return to these sample to look for this. A summary table of key characteristics noted in each experimental sample is shown in Table 8.

The MIND-project has received funding from the European Union's Euratom research and training program (Horizon2020) under grant agreement 661880.

Table 8. Summary table of key characteristics noted in each experimental sample.

Exp. No	Inoculated	Lactate	Dry density	Any colouration in initial cut	extensive later colouration	Fe enrichment of bentonite (SEM observations)	calcium enrichment	Aragonite	fibrous Fe	Fe 'polka-dots'in bentonite	Fe sulphides	Predominant interlayer cations at end of experiment (XRD)
BUG021	No	No	1.4	Not noted	Minimal but present	Yes, extensive	Yes, minimal	No	No	No	No	Predominantly divalent cations
BUG022	Yes	No	1.4	Not noted	strong, dark brown and ochre	Yes	Yes	Yes	Yes	No	No	Predominantly divalent cations
BUG023	No	Yes	1.4	No colouration noted in initial sample	strong, dark brown and ochre	Yes, minimal	Yes	Yes, minimal	No	No	No	Predominantly divalent cations
BUG024	Yes	Yes	1.4	No colouration noted in initial sample	strong, black and ochre	No	Yes	Yes	Yes	No	No	Contains both divalent and monovalent cations. Little change from starting material
BUG025	No	Yes	1.2	Slight green tinge in initial sample	strong, black and ochre	Yes, extensive	Yes	Yes	Yes	Yes	Yes	Approximately similar proportions of monovalent and divalent cations
BUG026	Yes	Yes	1.2	Green tinge in initial sample	strong, black and ochre	Yes, minimal	Yes	Yes, patchy	Yes	Yes	No	Contains both divalent and monovalent cations. Little change from starting material

The MIND-project has received funding from the European Union's Euratom research and training program (Horizon2020) under grant agreement 661880.

3.3 XRD analysis–summary of data previously presented in report D2.9 (Gregory *et al.*, 2018)

BUG021 uninoculated, 1400 kg m^{-3} no lactate added

The starting material and subsamples taken distal to the steel alteration produced a ≈12.5 Å smectite d_{001} spacing, suggesting the presence of predominantly monovalent (Na, K) interlayer cations. Material taken from the bentonite – steel interaction zone produced a larger ≈15.0 Å smectite d_{001} spacing, suggesting the presence of predominantly divalent (Ca, Mg, Fe) interlayer cations (Figure 25).

BUG022 inoculated, 1400 kg m^{-3} no lactate added

The starting material and subsamples taken distal to the steel alteration produced a ≈12.3 Å smectite d_{001} spacing, suggesting the presence of predominantly monovalent (Na, K) interlayer cations. Material taken from the bentonite – steel interaction zone produced a larger ≈14.0 Å smectite d_{001} spacing, suggesting the presence of predominantly divalent (Ca, Mg, Fe) interlayer cations (Figure 25).

BUG023 uninoculated, 1400 kg m^{-3} lactate added

The starting material and subsamples taken distal to the steel alteration produced a ≈12.3 Å smectite d_{001} spacing, suggesting the presence of predominantly monovalent (Na, K) interlayer cations. Material taken from the bentonite – steel interaction zone produced a larger ≈14.0 Å smectite d_{001} spacing, suggesting the presence of predominantly divalent (Ca, Mg, Fe) interlayer cations (Figure 25).

3.4 XRD analysis–full description of new data

3.4.1 BUG024 (1400 kg m^{-3} dry density, lactate added, inoculated)

The starting material and subsamples taken distal to the steel alteration produced a ≈12.5 Å smectite d_{001} spacing, suggesting the presence of predominantly monovalent (Na, K) interlayer cations. A low angle shoulder to these peaks at ≈14.0 Å suggests the presence of some divalent (Ca, Mg) interlayer cations (Figure 25). Unlike the previous experiments, material taken from the bentonite – steel interaction zone produced a similar peak profile suggesting more limited reaction than that noted in the BUG021, 022, 023 experiments (Figure 25).

3.4.2 BUG025 (1200 kg m^{-3} dry density, lactate added, uninoculated)

The starting material and subsamples taken distal to the steel alteration produced a ≈12.5 Å smectite d_{001} spacing, suggesting the presence of predominantly monovalent (Na, K) interlayer cations. A low angle shoulder to these peaks at ≈14.0 Å suggests the presence of some divalent (Ca, Mg) interlayer cations (Figure 25). Material taken from the bentonite – steel interaction zone produced a broad peak covering both ≈14.0 and 12.5 Å spacings suggesting approximately similar proportions of monovalent (Na, K) and divalent (Ca, Mg, Fe) interlayer cations (Figure 25).

3.4.3 BUG026 (1200 kg m^{-3} dry density, lactate added, inoculated)

The starting material and subsamples taken distal to the steel alteration produced a ≈12.5 Å smectite d_{001} spacing, suggesting the presence of predominantly monovalent (Na, K) interlayer cations (Figure 25). A low angle shoulder to these peaks at ≈14.0 Å suggests the presence of some divalent (Ca, Mg) interlayer cations (Figure 25). Material taken from the bentonite – steel interaction zone produced an approximately similar peak profile (as seen in the BUG024 experiment) suggesting little reaction compared to that noted in the BUG021, 022, 023 experiments (Figure 25).

The MIND-project has received funding from the European Union's Euratom research and training program (Horizon2020) under grant agreement 661880.

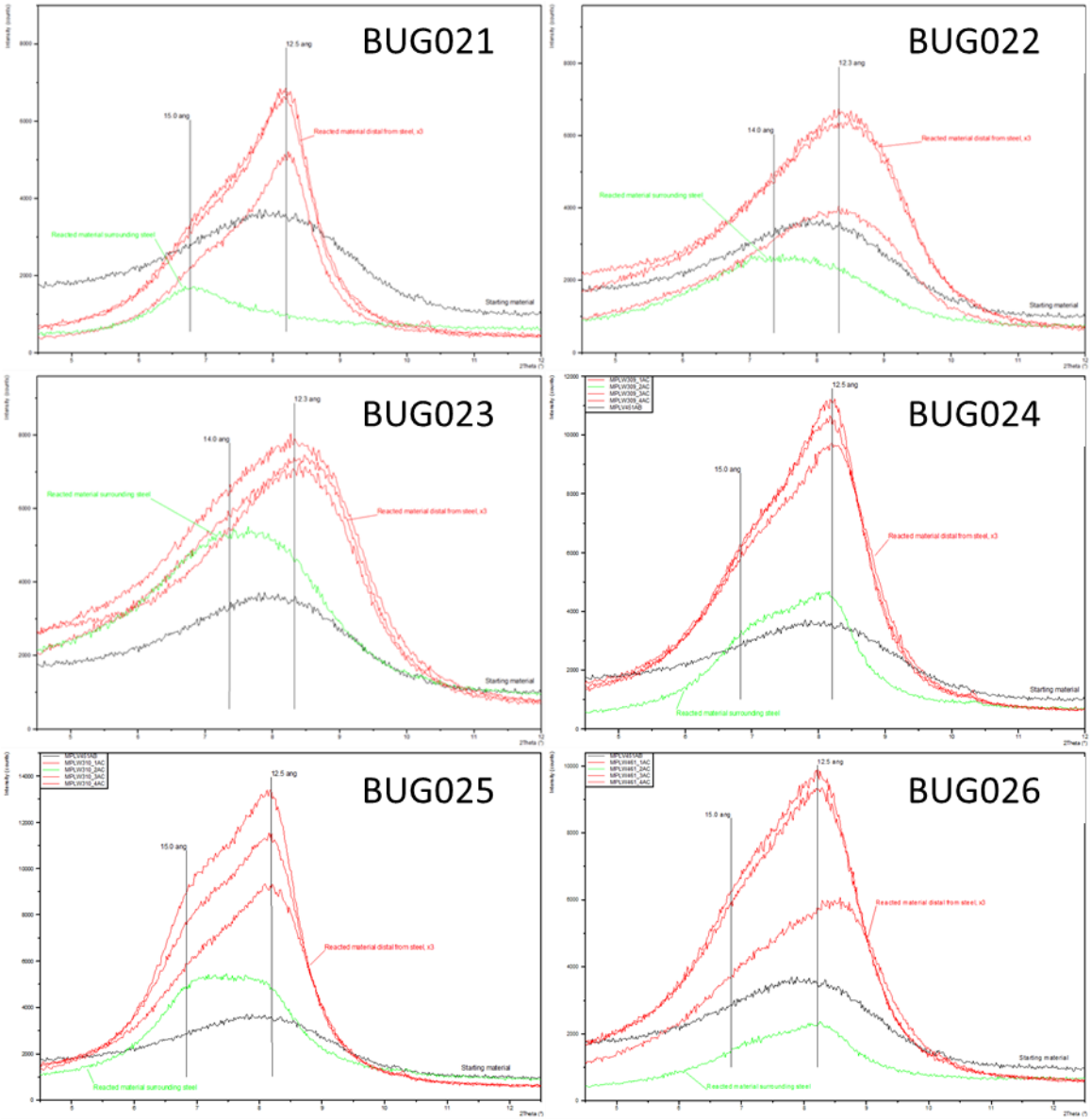

Figure 25 Zoomed view of low angle region of oriented mount XRD traces of starting material (black trace) and post experimental material from BUG024 (reacted material surrounding steel, green trace; reacted material distal from steel, red traces x3). Images on left are from uninoculated tests. Images on right are from inoculated tests.

3.5 Microbiological analysis

Anaerobic heterotrophs, aerobic heterotrophs, SRB were enumerated in all tests (BUG021- BUG026) (Figure 26). Samples of groundwater from the injection pump and the back-pressure pump were tested at the end of the experiment. No microbes were detected in any of the groundwater samples except in BUG022 when low levels of anaerobic heterotrophs were detected in groundwater from the injection pump (119 cells ml^{-1}) and aerobic heterotrophs were detected in groundwater from injection and back pressure pumps (305 and 62 cells ml^{-1}).

Anaerobic heterotrophs were detected in all subsamples of bentonite from inoculated tests (BUG022, BUG024, BUG026) with no obvious pattern associated with distribution throughout the sample or relationship to the location of the steel. The mean anaerobic heterotroph cell counts per g bentonite was highest in BUG022 (1.7×10^6 cells g^{-1}) compared to 3.1×10^5 cells g^{-1} in BUG026 and 1.0×10^5 cells g^{-1} in BUG024. The same pattern in cell density was observed for aerobic heterotrophs with the highest cell densities observed in BUG022 (4.6×10^4 cells g^{-1}), followed by BUG026 (1.6×10^4 cells g^{-1}) and BUG024 (7.8×10^{-3} cells g^{-1}). In BUG022 and BUG024 the number of viable anaerobic

The MIND-project has received funding from the European Union's Euratom research and training program (Horizon2020) under grant agreement 661880.

heterotrophs increased during the course of the experiment, but decreased in BUG026. While conducting MPN counts for heterotrophs in the first pair of experiments (BUG021 and BUG022), difficulties were experienced distinguishing between cloudiness caused by the presence of clay and cloudiness as the diagnostic feature of heterotrophic growth. Due to this risk of scoring false positives, later tests used a plate count method (Miles Misra) for enumeration. Therefore, the heterotrophic cell counts recorded in BUG021 and BUG022 should be treated with caution.

There were problems with the MPN tests for SRB in BUG025 and BUG026, with contamination of negative controls and the production of black precipitates in iron-reducing assay. Therefore, data on these groups is not available for these tests. In BUG021 – BUG024, SRB were only detectable in the inoculated tests. Mean cell density in the bentonite was relatively low (500 cells g^{-1} in BUG022, 781 cells g^{-1} in BUG 024). This represents an increase in number of cells compared to the starting density in inoculated in the bentonite sample (note that values for inoculum in Figure 26 have been adjusted to give a cell count per g bentonite).

The MIND-project has received funding from the European Union's Euratom research and training program (Horizon2020) under grant agreement 661880.

A. Anaerobic heterotrophs

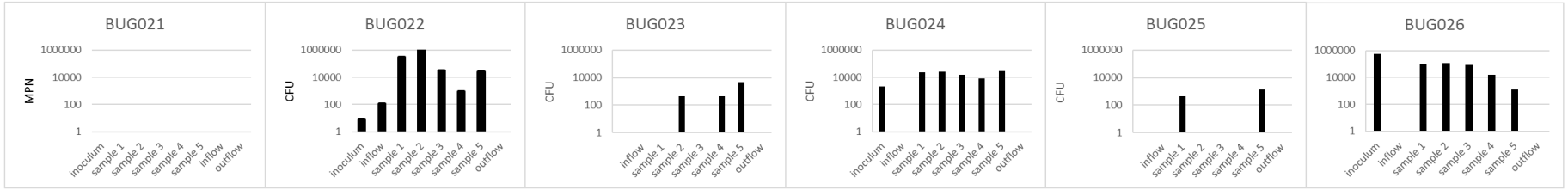

B. Aerobic heterotrophs

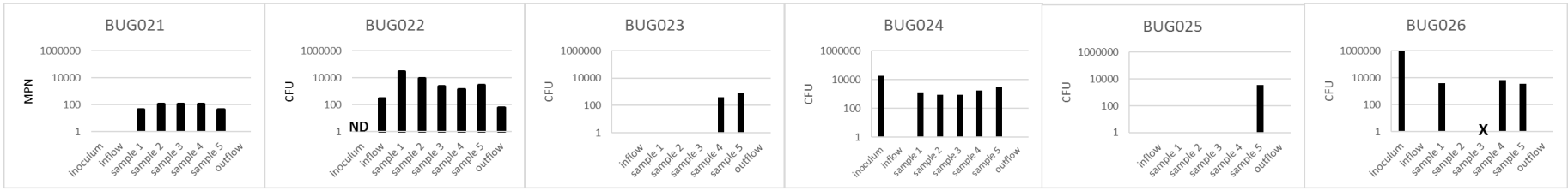

C. Sulphate reducing bacteria

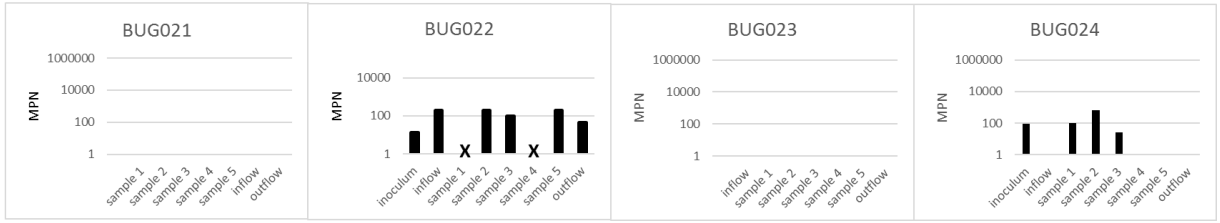

Figure 26 Enumeration of bacteria in inocula, groundwater samples and bentonite samples. Refer to figure 5b for location of samples 1-5. N.B. heterotrophs in BUG021 and BUG022 were counted by MPN, for other tests Miles Misra technique was used. ND=not determined. X= invalid test result either due to entry outside of range of MPN algorithm or no dilution with countable colonies. No data shown for BUG205 or BUG026 SRB due to contamination of negative controls..

The MIND-project has received funding from the European Union's Euratom research and training program (Horizon2020) under grant agreement 661880.

4 Discussion

A series of tests have been carried out on the interactions between bentonite, steel and microorganisms in flow experiments designed to replicate some of the conditions surrounding a geological disposal facility. Data from these experiments have been discussed in this, and a previous report (Gregory *et al.*, 2018). A comparison of all samples can now be made from three uninoculated and three inoculated tests.

To test the potential impact of microbial activity on clay alteration and steel corrosion, an initial dry density of bentonite of 1400 kg m^{-3} was selected (calculated dry wet densities of 1834 kg m^{-3} to 1864 kg m^{-3} (Table 1). This density represents a value close to the upper reported limits for microbial survival in bentonite, which has been reported to be in the region of 1250 kg m^{-3} – 1600 kg m^{-3} dry density (or 1900 to 2100 kg m^{-3} wet density). It is slightly lower than the proposed dry density of buffer included in different national repository concepts, which range from around 1450 kg m^{-3} – 1650 kg m^{-3} (Sellin and Leupin, 2014). This density was selected because if microbial survival or activity could not be detected at this density, it would provide some confidence that there would be no microbial activity at the recommended in situ densities (assuming that the bentonite was full hydrated and homogenised).

In the first two pairs of tests, samples were prepared to a dry density of 1400 kg m^{-3} and in each case an uninoculated sample was compared to an inoculated one. The only difference between these pairs was that the second pair (BUG023 and BUG024) were amended by the addition of lactate to the groundwater used to prepare and hydrate the samples, and used to fill the injection pump. In the samples without lactate (BUG021 and BUG022) any microbial activity would need to rely on traces of organic carbon from the clay or hydrogen (e.g. generated by steel corrosion) as electron donors. The organic carbon contained within clays is considered to be recalcitrant and not readily used by microorganisms (Leupin *et al.*, 2017). The lactate was added to the second pair of tests to provide an additional electron donor to support microbial activity. Lactate is one of a number of carbon compounds that SRB can use as an electron donor (Muyzer and Stams, 2008) and is frequently used in experiments investigating sulphate reducing activity in bentonites in a GDF context (Masurat *et al.*, 2010a, 2010b; Pedersen, 2010; Maia *et al.*, 2016). In the uninoculated sample of each pair, limited bacteria (aerobic and anaerobic heterotrophs) were detected in the uninoculated sample, with greater numbers of these organisms detected in the inoculated sample. In BUG021 low numbers of SRB were detected in all portions of the sample. All of the three microbial groups tested (anaerobic- and aerobic heterotrophs and SRB) were identified in BUG022, at much higher numbers, throughout the sample and in both pumps at the end of the experiment. Comparison of the concentration of organisms added to the sample in the inoculation from the enrichment culture and the mean cell concentration in the post experimental sample indicates that all four groups of microorganisms were able to multiply during the experiment. In BUG024, there was a slight increase in the number of anaerobic heterotrophs and sulphate-reducing bacteria but the number of aerobic heterotrophs. The drop in the number of aerobes might be expected due to the anoxic conditions in the experiment. Although the species of SRB present was not analysed in these experiments, *Desulfotomaculum* species have been identified as the dominant species in FEBEX bentonite (Haynes *et al.*, 2018). These organisms are particularly resistant to high pressure, which may be why SRB were found in these tests, even though they were compressed to densities normally considered to be at the upper limits of survival of SRB.

Unexpectedly, the total recorded cell numbers were considerably lower in the inoculated test (BUG024) containing lactate compared to the non-lactate test (BUG022), suggesting that the sodium lactate did not increase the microbial activity in these samples. However, in comparing the microbial data from the first pair of tests to later ones, care must be taken as the method used for enumeration was changed from MPN to Miles Misra due to concerns of over-estimating the number of organisms when using the former. The reason for this was that the positive test for growth in this

The MIND-project has received funding from the European Union's Euratom research and training program (Horizon2020) under grant agreement 661880.

MPN assay is cloudiness of PTYG medium caused by microbial growth. Unfortunately, it was noted that the bentonite clouds the medium even without microbial growth leading to difficulty in interpretation.

In all tests, the groundwater was sterilised before use in the experiment. Although it was anticipated that some microbial growth might be seen in the back-pressure pump (outflow) of inoculated tests as it contains fluid that has flowed through the inoculated core, it was hoped that the fluid in the upstream injection pump (inflow) would remain sterile. The data show some evidence of movement of bacteria from the sample to the back-pressure fluid in the first inoculated tests (with bacteria detected in both the inflow and outflow of BUG022). No microbes were detected in inflow or outflow samples of later tests. This may reflect the fact that in between tests after BUG021 and BUG022, the apparatus was filled with 70% methanol at a pressure of 1MPa, which will have forced the methanol into all parts of the system allowing more effective sterilisation. The detection of microorganisms in uninoculated tests might reflect small amounts of cells getting into the system, ether during the lengthy sample preparation process or the subsampling process. Both activities were carried out in an anaerobic chamber to retain viability of oxygen sensitive species. Care was taken to limit exposure of the sample to the atmosphere in the anaerobic chamber, and results suggest that while this was not 100% effective at excluding microorganisms, contamination could be kept to a minimum.

SEM analysis of the 1400 kg m^{-3} tests revealed variability in the amount of alteration to the bentonite and steel. In all four samples enrichment of calcium in bentonite surrounding the corroding steel was observed. Precipitated acicular calcium carbonate crystals (probably aragonite) were commonly observed in fracture space around the steel in both of the inoculated samples, but were observed only rarely in the uninoculated test BUG023 and not at all in uninoculated BUG021. Enrichment of iron within the bentonite around the steel, with iron coating (of replacing bentonite) was observed in tests (BUG021 - BUG023), but fibrous iron was observed around the corroded steel only in the inoculated samples. The presence of crystals growing into open space within fractures indicates that these fractures were open during the experiment, consistent with cracks opening up around corroding steel as water within the bentonite is consumed by the corroding steel causing the clay to shrink back (Milodowski *et al.*, 2009; Smart *et al.*, 2017). As seen in other studies (Milodowski *et al.*, 2007, 2009), it is proposed that Fe from the corroding steel displaced the Ca^{2+} from the exchangeable cation interlayer sites in the montmorillonite and that aragonite formed as more Ca^{2+} was displaced from the bentonite and was concentrated at the leading edges of the diffusive Fe fronts as Fe migrated away from the steel and into the bentonite matrix. It is not clear what effect the observed aragonite crystal growth might have on the swelling properties of the bentonite, but other changes observed from temperature and humidity-controlled, oriented mount XRD analysis of samples from the first three experiments (BUG021, BUG022 and BUG023) could indicate that the corrosion of steel within the clay could reduce the swelling capacity of the clay through the replacement of monovalent cations by divalent cations which was observed in the stained zone but not the starting material and the bentonite subsamples taken further away from this stained zone. However, this change was less pronounced in the BUG024. Although this shift in basal spacing is commonly observed, this is not always the case and it is not unheard of for related samples to behave differently (e.g. Smart *et al.*, 2017).

The swelling pressure generated by BUG021 was lower than the swelling pressure of all other 1400 kg m^{-3} dry density tests. The data suggest that this may be due to unintentional “pre-stressing” of tests BUG022 and BUG024. Similar mean permeability was detected in these tests, but the inoculated sample consistently showed a slightly lower permeability.

The results from the four 1400 kg m^{-3} samples indicated that bacteria were able to survive and grow in these conditions and suggested that there might be a link between the presence of bacteria and the fibrous iron and aragonite crystals observed in the fracture space around the corroding steel. Despite these differences in the characterisation of the material, there was no discernible changes in the swelling pressures generated by these samples over the course of the experiment. One of the key

The MIND-project has received funding from the European Union’s Euratom research and training program (Horizon2020) under grant agreement 661880.

aims of these experiments was to identify whether the presence and activity of microorganisms interacting with steel and clay was sufficient to change the swelling behaviour, and hence performance of the bentonite buffer material. The XRD data indicated changes that could affect swelling capacity, but this could not be detected by our experimental set-up. In order to explore whether this apparatus could be used to detect changes in swelling pressure if the microbial activity was higher, the third pair of experiments were run using samples prepared to a lower dry density of 1200 kg m^{-3}, with lactate was added to the groundwater as before. It was anticipated that the lower dry density would encourage microbial activity as has previously been reported (Masurat *et al.*, 2010b; Pedersen, 2010; Bengtsson and Pedersen, 2017; Bengtsson *et al.*, 2017). In the inoculated test, the lower density led to much higher numbers of heterotrophs being recorded in inoculated BUG026 compared to the higher density inoculated BUG024. Unfortunately, problems with contamination of MPN counts for SRB meant that no data could be obtained for these groups. Due to the limitations of these culture methods, it was intended to apply DNA based techniques to quantify and characterise the microbial community. However, bentonite is a notoriously difficult material to extract DNA from, and despite modifications to protocols described in the methods, it was not possible to obtain DNA for PCR amplification. DNA extraction techniques based on the phenol chloroform technique are being applied in the hope of obtaining further data from this material.

Examination of BUG025 by SEM showed the greatest amount of alteration of all the samples analysed, with dense secondary phases coating the surface of the clay, considerable iron precipitation (including fine-grained iron phases) and abundant aragonite. Elemental mapping showed the presence of Fe-oxide and fibrous Fe-S phases. This was the only sample to contain secondary Fe-S phases. In contrast to previous tests, the inoculated BUG026 had less evidence of alteration with patchier aragonite precipitation, and minimal iron enrichment of the bentonite. Additionally, an iron “polka dot” feature was observed in both BUG025 and BUG026. The first two pairs of experiments suggested that formation of aragonite and Fe enrichment of bentonite surrounding corroding steel is more extensive in the presence of microorganisms in the sample. The data from BUG025 and BUG026 suggests a more complex relationship. Calcium and iron enrichment, along with the fibrous iron around the corroding steel were observed in both samples, but aragonite crystals were sparse in the inoculated BUG026 polished block and more common in the uninoculated sample. Despite greater alteration being observed under SEM, XRD data from these sample showed less alteration to the predominant cations, compared to BUG021-BUG023. Inoculated samples BUG024 and BUG026 showed the least change from the starting material of all sample, while uninoculated BUG025 showed an intermediate degree of cation displacement. While this is inconsistent with earlier samples in this study, it is consistent with XRD of the bentonite clay in previous work (e.g. Smart *et al.*, 2017) where little change in the bentonite mineralogy was associated with corroding steel.

The low-density pair also had the greatest difference between the two samples in terms of permeability. Permeability of both samples was much higher than the previous samples, reflecting the lower dry density, but interestingly the permeability of the inoculated sample is much lower. This lower permeability between the inoculated sample compared to its uninoculated partner is observed in all samples (including BUG027 and BUG028, for which only the logging data is presented here), but the difference was very subtle in all 1400 kg m^{-3} samples. In contrast a 20% difference between BUG025 and BUG026 was observed. It might be speculated that this could be due to increased microbial number and activity in lower density samples. As discussed previously, no data are available on the numbers of SRB in these samples, which is unfortunate due to the association of these organisms with enhanced corrosion. The heterotroph plate counts do indicate that the overall number of bacteria in BUG026 is considerably higher than the number in the similar sample with higher dry density (BUG024). Despite the largest change in permeability, and the abundance of microorganisms, it is interesting to note that the sample which had the largest visible alteration of steel and bentonite was the uninoculated (BUG025) sample, suggesting other non-biological factors are also important.

The MIND-project has received funding from the European Union’s Euratom research and training program (Horizon2020) under grant agreement 661880.

Bentonite around the steel in BUG025 and BUG026 (and to a lesser extent BUG023 and BUG024) displayed a greenish tinge on being cut open. After removal from the vacuum bags, prior to analysis, the samples displayed a prominent brown-ochre coloured halo around the steel filings. One possibility for this would be the presence of 'green-rust', layered Fe^{II}-Fe^{III} hydroxides (O'Loughlin *et al.*, 2003). Green-rust is an unstable corrosion product which can be formed by a number of abiotic and biotic processes under circumneutral to alkaline conditions in suboxic environments (O'Loughlin *et al.*, 2003). Green rust is a crystalline mineral containing iron (II) and iron (III) cations, the hydroxide anion and another cation, typically carbonate (CO_3^{2-}), chloride (Cl^-) or sulphate (SO_4^{2-}) *e.g.* $(Fe_4\ (II)Fe_2(III)(OH)_{12}SO_4 \cdot 8H_2O$, in a layered double hydroxide series. Depassivation of steel to form green rust typically occurs when the ratio of concentration of chloride ions to hydroxide ions is greater than 1 (for example in seawater). Exposure to air for a short time (a few minutes), is sufficient to transform the ferric phases within the green rust to Fe oxyhydroxides, including ferrihydrite, goethite, lepidocrocite or magnetite (Simon *et al.*, 2003; Sumoondur *et al.*, 2008). Due to this rapid oxidation, it is extremely difficult to confirm the presence of green rust by traditional analytical methods. Successful studies into the mechanisms of green rust sulphate (GR-SO_4) have monitored the reaction by advance techniques such as combining time-resolved synchrotron-based wide-angle X-ray scattering (WAXS) with highly controlled chemical synthesis and electrochemical (Eh and pH) monitoring (Ahmed *et al.*, 2010), X-ray absorption spectroscopy (XAS) including X-ray absorption near edge structure (XANES) and X-ray absorption fine structure (EXAFS) (O'Loughlin *et al.*, 2003), or synchrotron based XAS, Mössbauer spectroscopy and TEM (Pantke *et al.*, 2012). Green rust has been reported in association with corrosion in bentonite *e.g.* (Carlson *et al.*, 2007).

Data from the first two pairs of tests presented here suggested that the presence of bacteria in samples influenced the changes observed in the clay, in particular in relation to the presence of aragonite and fibrous iron in inoculated samples. However, later experiments, when the density of samples was reduced, and where there were more heterotrophic bacteria, these differences were not observed. It is therefore difficult to identify a consistent effect of microbes on the corrosion of steel and the impact on the surrounding bentonite. Although effort was made to ensure uniformity (e.g. homogeneity of compressed bentonite within a sample and uniformity between samples), it may be that our observations simply reflect the heterogeneity of samples and experimental error. On the other hand, we may be detecting a subtle, but important, influence of microorganisms. The experimental set-up employed in these experiments, was designed to create the most realistic representation of *in situ* conditions as possible, but this leads to somewhat complex experiments. This, combined with the relatively long run time of experiments, and limited number of apparatus, meant that replication of samples was not possible. However, tests BUG027 and BUG028, for which only continuous logging data has been presented here, replicate the conditions in BUG023 and BUG024 (1400 kg m^{-3}, lactate added) and should provide an insight into the heterogeneity of materials and conditions used and reproducibility of results.

The challenge of quantifying changes to safety case critical parameter (such as loss of swelling capacity) in realistic flow experiments remains.

Despite the fact that the observed changes (particularly in the XRD) would suggest that swelling capacity could be reduced during the course of most of the experiments, loss of swelling pressure was not seen; while there was some noise in the swelling pressure data, a number of tests exhibit marginally higher swelling pressure values at the end of the test phase. By cross-plotting the swelling pressure and permeability data against the estimated bulk density of the core (Table 1) it is possible to discern some general trends in behaviour (Figure 7). As expected, the data showed that swelling pressure and permeability are linked to the density of the sample and that swelling pressures increase slightly as the duration of the test increases. This suggests hydration and homogenisation of the clay continued throughout the experiment. However, no correlation between swelling pressure and the inoculation state of the sample is evident which probably reflects limitations in the number and positioning of load cells and/or the resolution of the measurement system and its ability to

The MIND-project has received funding from the European Union's Euratom research and training program (Horizon2020) under grant agreement 661880.

detect subtle changes in stress as samples continued to hydrate and homogenise. Of more importance are the changes in permeability between inoculated and non-inoculated samples which is also clearly evident in Figure 7. The change in permeability observed between BUG025 and BUG026 far exceeds that which might be expected by the small change in density between the two test samples. The fact that bulk density is not the driving force for the changes in permeability between paired experimental samples is borne out by tests BUG023 and BUG024. Here, even though BUG023 has a slightly higher density than BUG024, and should therefore exhibit a lower permeability, the inoculated sample BUG024 exhibits a lower permeability.

The novelty of these reactive flow experiments is in the coupling of biological, chemical and physical processes, particularly the use of load cells to measure biogeochemically induced changes in swelling pressure through enhanced metal corrosion. Tying microbiological activity to the properties of clay is critical for the safety case and understanding the impact of microbes on the hydromechanical properties of bentonite remains an unanswered question. While the data presented show the potential importance of microbial activity on the evolution of bentonite permeability, further testing is required. These tests should be performed over extended durations, to fully quantity this behaviour, and importantly, its coupling to pressure stresses. While no correlation in the latter was observed, it is highly likely given the data from XRD and SEM analysis, that changes in swelling pressure would have occurred if tests could be run for sufficient time, or if a different steel to bentonite ratio was used. Data from these experiments has not shown any change in swelling pressure caused by microbe-steel-bentonite interactions. The ability to detect loss of swelling capacity in real time in laboratory experiments would be a useful tool to assess the impacts of coupled biological, chemical and physical processes on swelling capacity. This sort of technique has been successfully deployed to investigate changes in swelling pressure caused by increases and decreases in porewater pressure, desaturation, salinity and gas injection. With further development this technique could be used to monitor corrosion induced loss of swelling capacity. Carefully calibrated experiments would allow the calculation of loss in swelling pressure per unit area of corroding steel. Such a technique could be widely applied to radioactive waste research, not just microbial effects.

Given these findings, many aspects of how microbial activity alters the hydraulic behaviour of bentonite remains unanswered. An association of reduced permeability of the clay has been observed, but no mechanism for this has been identified. These observations deserve further investigation will be the focus of future tests involving higher iron:bentonite ratio and longer test durations.

SUMMARY

These experiments have investigated the influence of microbial activity on the physical properties of bentonite and steel. Some of the main observations are as follows

- Previous reports of higher in microbial survival in lower density bentonite samples have been confirmed for FEBEX bentonite, with survival and growth detected in samples with an initial dry density of 1200 kg m^{-1} and 1400 kg m^{-3}. This indicates that in FEBEX bentonite microorganisms survive at the upper range of quoted dry densities for bentonites
- The first two pairs of tests (each consisting on one inoculated and one uninoculated sample) suggested that the presence of microorganisms is associated with particular iron phases and the development of aragonite crystals. However, the lower density experiments did not show this pattern.
- The basal spacing of bentonite increased during experiments, indicating replacement of monovalent cations by divalent ones in experiments BUG021- BUG023, but again the lower density experiments did not show this same pattern.
- In all tests, permeability was lower in the inoculated sample, and in the low-density tests (1200 kg m^{-3}) a 20% reduction in permeability was observed in inoculated samples.

The MIND-project has received funding from the European Union's Euratom research and training program (Horizon2020) under grant agreement 661880.

5 Acknowledgement

The MIND-project has received funding from the European Union's Euratom research and training program (Horizon2020) under grant agreement 661880 The MIND-project.

6 References

Ahmed, I.A.M., Benning, L.G., Kakonyi, G., Sumoondur, A.D., Terrill, N.J., and Shaw, S. (2010) Formation of green rust sulfate: A combined in situ time-resolved X-ray scattering and electrochemical study. *Langmuir*.

Bagnoud, A., Chourey, K., Hettich, R.L., de Bruijn, I., Andersson, A.F., Leupin, O.X., et al. (2016) Reconstructing a hydrogen-driven microbial metabolic network in Opalinus Clay rock. *Nat. Commun.* **7**: 12770.

Bengtsson, A., Blom, A., Johansson, L., Taborowski, T., Eriksson, L., and Pedersen, K. (2017) Bacterial sulphide-producing activity in water saturated iron-rich Rokle and iron-poor Gaomiaozi bentonite at wet densities from 1750 to 1950 kg m^{-3} SKB Technical Report TR-17-05.

Bengtsson, A. and Pedersen, K. (2017) Microbial sulphide-producing activity in water saturated Wyoming MX-80, Asha and Calcigel bentonites at wet densities from 1500 to 2000kgm^{-3}. *Appl. Clay Sci.* **137**: 203–212.

Boivin-Jahns, V. and Ruimy, R. (1996) Bacterial diversity in a deep-subsurface clay environment. *Appl. Environ. Microbiol.* **62**: 3405–3412.

Carlson, L., Karnland, O., Oversby, V.M., Rance, A.P., Smart, N.R., Snellman, M., et al. (2007) Experimental studies of the interactions between anaerobically corroding iron and bentonite. *Phys. Chem. Earth* **31**: 334–345.

Cui, K., Sun, S., Xiao, M., Liu, T., Xu, Q., Dong, H., et al. (2018) "Microbial mineral illization of montmorillonite in low-permeability oil reservoirs for microbial enhanced oil recovery. *Appl. Environ. Microbiol.* **84**: e00176-18.

Deniau, I., Derenne, S., Beaucaire, C., Pitsch, H., and Largeau, C. (2001) Morphological and chemical features of a kerogen from the underground Mol laboratory (Boom Clay Formation, Oligocene, Belgium): structure, source organisms and formation pathways. *Org. Geochem.* **32**: 1343–1356.

Esnault, L., Libert, M., Bildstein, O., Mustin, C., Marsal, F., and Jullien, M. (2013) Impact of iron-reducing bacteria on the properties of argillites in the context of radioactive waste geological disposal. *Appl. Clay Sci.* **83–84**: 42–49.

Féron, D. and Crusset, D. (2014) Microbial induced corrosion in French concept of nuclear waste underground disposal. *Corros. Eng. Sci. Technol.* **49**: 540–547.

Gould, W.D., Stichbury, M., Francis, M., Lortie, L., and Blowes, D.W. (2003) An MPN method for the enumeration of iron-reducing bacteria. *Proc. Min. Environ. III. Laurentian Univ. Sudbury, ON, Canada*.

Gregory, S., Barnett, M., Field, L., and Milodowski, A. (2019) Subsurface Microbial Hydrogen Cycling: Natural Occurrence and Implications for Industry. *Microorganisms*.

Gregory, S., Green, K., Harrington, J., Field, L.F., Kemp, S., and Bateman, K. (2018) Evolution of stress in biotic and abiotic clay flow cells. MIND project deliverable 2.9.

Hajj, H. El, Abdelouas, A., Grambow, B., Martin, C., and Dion, M. (2010) Microbial corrosion of P235GH steel under geological conditions. *Phys. Chem. Earth, Parts A/B/C* **35**: 248–253.

Haynes, H.M., Pearce, C.I., Boothman, C., and Lloyd, J.R. (2018) Response of bentonite microbial communities to stresses relevant to geodisposal of radioactive waste. *Chem. Geol.*

The MIND-project has received funding from the European Union's Euratom research and training program (Horizon2020) under grant agreement 661880.

Högfors-Rönnholm, E., Christel, S., Engblom, S., and Dopson, M. (2018) Indirect DNA extraction method suitable for acidic soil with high clay content. *MethodsX* **5**: 136–140.

Humphreys, P., West, J.W., and Metcalfe, R. (2010) Microbial effects on repository performance.

ICDD (2018) PDF-4+ 2018 (Database). In Soorya Kabekkodu, Ed., International Centre for Diffraction Data, Newtown Square, Pennsylvania, U.S.A.

ICDD (2019) PDF-4+ 2019 (Database). In Soorya Kabekkodu, Ed., International Centre for Diffraction Data, Newtown Square, Pennsylvania, U.S.A.

Kostka, J.E., Haefele, E., Viehweger, R., and Stucki, J.W. (1999) Respiration and Dissolution of Iron(III)-Containing Clay Minerals by Bacteria. *Environ. Sci. Technol.* **33**: 3127–3133.

Leupin, O.X., Bernier-Latmani, R., Bagnoud, A., Moors, H., Leys, N., Wouters, K., and Stroes-Gascoyne, S. (2017) Fifteen years of microbiological investigation in Opalinus Clay at the Mont Terri rock laboratory (Switzerland). *Swiss J. Geosci.* **110**: 343–354.

Libert, M., Kerber-Schütz, M., Esnault, L., and Bildstein, O. (2013) Are Underground Clay Disposal Conditions Favorable for Microbial Activity and Biocorrosion? *Procedia Earth Planet. Sci.* **7**: 73–76.

Lopez-Fernandez, M., Cherkouk, A., Vilchez-Vargas, R., Jauregui, R., Pieper, D., Boon, N., et al. (2015) Bacterial Diversity in Bentonites, Engineered Barrier for Deep Geological Disposal of Radioactive Wastes. *Microb. Ecol.*

Maia, F., Puigdomenech, I., and Molinero, J. (2016) Modelling rates of bacterial sulfide production using lactate and hydrogen as energy sources Technical Report TR-16-05.

Masurat, P., Eriksson, S., and Pedersen, K. (2010a) Evidence of indigenous sulphate-reducing bacteria in commercial Wyoming bentonite MX-80. *Appl. Clay Sci.* **47**: 51–57.

Masurat, P., Eriksson, S., and Pedersen, K. (2010b) Microbial sulphide production in compacted Wyoming bentonite MX-80 under in situ conditions relevant to a repository for high-level radioactive waste. *Appl. Clay Sci.*

Milodowski, A.E., Cave, M.R., Kemp, S.J., Taylor, H., Vickers, B.P., Green, K.A., et al. (2007) Mineralogical investigations of the interaction between iron corrosion products and bentonite form the NF-PRO experiments (Phase 1) SKB Techical Report TR-09-03.

Milodowski, A.E., Cave, M.R., Kemp, S.J., Taylor, H., Vickers, B.P., Green, K.A., et al. (2009) Mineralogical investigations of the interaction between iron corrosion products and bentonite from the NF-PRO Experiments (Phase 1) (2009) Svensk Kärnbränslehantering AB Technical Report TR-09-02.

Motamedi, M., Karland, O., and Pedersen, K. (1996) Survival of sulfate reducing bacteria at different water activities in compacted bentonite. *FEMS Microbiol. Lett.* **141**: 83–87.

Mulligan, C., Yong, R., and Fukue, M. (2009) Some effects of microbial activity on the evolution of clay-based buffer properties in underground repositories. *Appl. Clay Sci.* **42**: 331–335.

Muyzer, G. and Stams, A.J.M. (2008) The ecology and biotechnology of sulphate-reducing bacteria. *Nat. Rev. Microbiol.* **6**: 441–454.

O'Loughlin, E., Kelly, S.D.., Cook, R.E., Csencsits, R., and Kemner, K.M. (2003) Reduction of Uranium (VI) by mixed iron(II)/Iron(III) hydroxide (green rust): Formation of UO2 nanoparticles. *Environ. Sci. Technol.* **31**: 721–727.

Pantke, C., Obst, M., Benzerara, K., Morin, G., Ona-Nguema, G., Dippon, U., and Kappler, A. (2012) Green rust formation during Fe(II) oxidation by the nitrate-reducing acidovorax sp. strain BoFeN1. *Environ. Sci. Technol.*

The MIND-project has received funding from the European Union's Euratom research and training program (Horizon2020) under grant agreement 661880.

Pedersen, K. (2010) Analysis of copper corrosion in compacted bentonite clay as a function of clay density and growth conditions for sulfate-reducing bacteria. *J. Appl. Microbiol.*

Pedersen, K., Motamedi, M., Karnland, O., and Sanden, T. (2000) Mixing and sulphate-reducing activity of bacteria in swelling, compacted bentonite clay under high-level radioactive waste repository conditions. *J. Appl. Microbiol.* **89**: 1038–1047.

Perdrial, J.N., Warr, L.N., Perdrial, N., Lett, M.-C., and Elsass, F. (2009) Interaction between smectite and bacteria: Implications for bentonite as backfill material in the disposal of nuclear waste. *Chem. Geol.* **264**: 281–294.

Postgate, J.R. (1979) The sulphate-reducing bacteria. CUP Archive.

Rajala, P., Bomberg, M., Vepsäläinen, M., and Carpén, L. (2017) Microbial fouling and corrosion of carbon steel in deep anoxic alkaline groundwater. *Biofouling* 1–15.

Rajala, P., Carpén, L., Vepsäläinen, M., Raulio, M., Sohlberg, E., and Bomberg, M. (2015) Microbially induced corrosion of carbon steel in deep groundwater environment. *Front. Microbiol.* **6**: 647.

Sellin, P. and Leupin, O.X. (2014) The use of clay as an engineered barrier in radioactive-waste management - A review. *Clays Clay Miner.*

Simon, L., François, M., Refait, P., Renaudin, G., Lelaurain, M., and Génin, J.M.R. (2003) Structure of the Fe(II-III) layered double hydroxysulphate green rust two from Rietveld analysis. *Solid State Sci.*

Smart, N.R., Reddy, B., Rance, A.P., Nixon, D.J., Frutschi, M., Bernier-Latmani, R., and Diomidis, N. (2017) The anaerobic corrosion of carbon steel in compacted bentonite exposed to natural Opalinus Clay porewater containing native microbial populations. *Corros. Eng. Sci. Technol.* **52**: 110–112.

Stroes-Gascoyne, S., Hamon, C.J., Maak, P., and Russell, S. (2010) The effects of the physical properties of highly compacted smectitic clay (bentonite) on the culturability of indigenous microorganisms. *Appl. Clay Sci.* **47**: 155–162.

Stroes-Gascoyne, S. and West, J.M. (1997) Microbial studies in the Canadian nuclear fuel waste management program. *FEMS Microbiol. Rev.* **20**: 573–590.

Sumoondur, A., Shaw, S., Ahmed, I., and Benning, L.G. (2008) Green rust as a precursor for magnetite: an in situ synchrotron based study. *Mineral. Mag.*

Urios, L., Marsal, F., Pellegrini, D., and Magot, M. (2012) Microbial diversity of the 180 million-year-old Toarcian argillite from Tournemire, France. *Appl. Geochemistry* **27**: 1442–1450.

Wouters, K., Moors, H., Boven, P., and Leys, N. (2013) Evidence and characteristics of a diverse and metabolically active microbial community in deep subsurface clay borehole water. *FEMS Microbiol. Ecol.* **86**: 458–473.

The MIND-project has received funding from the European Union's Euratom research and training program (Horizon2020) under grant agreement 661880.